

## Chapter 2

# Heat Conduction and Thermal Parameters

**Abstract** This chapter presents the basic equations for conductive heat transfer and the main thermal parameters of the rocks, in particular the thermal conductivity and radiogenic heat. Also, it outlines the most commonly used techniques for estimating these parameters. Models involving the application of mixing laws for a mineral aggregate are discussed together with techniques for estimating the in situ thermal conductivity and volumetric heat capacity. Finally, methods for determining the radiogenic heat in the crust are introduced.

**Keywords** Conductive heat flow • Thermal properties • Thermal conductivity measurements • Radiogenic heat • Laboratory and ground gamma-ray spectrometry

## 2.1 Physical Parameters

It is well known that the heat transfer by conduction prevails in the lithosphere. The equations governing heat conduction include physical parameters such as thermal conductivity, thermal diffusivity and radiogenic heat. In a steady-state thermal regime, i.e. when temperature does not vary with time, thermal conductivity expresses how early heat is transported due to a spatial variation in temperature. Under transient heat conduction, thermal diffusivity describes the rate at which heat flows. Radiogenic heat is produced by naturally occurring radioactive elements, whose decay involves the conversion of mass into energy.

### 2.1.1 Thermal Properties

Fourier's law states that in isotropic solids the thermal conductivity  $k$  is a constant of proportionality between heat-flow density  $q$  and temperature gradient  $\nabla T$

$$q = -k \nabla T \quad (2.1)$$

where the minus sign indicates that heat propagates in the direction of the decreasing temperature. Since  $q$  is the amount of energy flowing through a unit area per unit time,  $k$  is expressed in  $\text{W m}^{-1} \text{K}^{-1}$ . In the lithosphere, there are three mechanisms which contribute to thermal conductivity: (i) the diffusion of heat by phonon propagation (lattice conductivity  $k_l$ ), (ii) the transfer of heat through emission and absorption of photons (radiative conductivity  $k_r$ ) and (iii) the transport of energy by quasiparticles composed of electrons and positive holes (exciton conductivity  $k_e$ ), whose contribution, however, is negligible in the lithosphere. Thus,  $k$  results formed from the sum of the lattice conductivity and radiative conductivity.

At low temperatures, the diffusion of thermal vibrations is the mechanism that essentially contributes to the rock thermal conductivity. In this case, for a single isotropic crystal, at temperatures above the Debye temperature,  $k_l$  is given by (Lawson 1957)

$$k_l = \frac{a_i K^{3/2}}{3 \gamma^2 T \rho^{1/2}} \quad (2.2)$$

where  $a_i$  is the interatomic distance,  $K$  is the bulk modulus,  $T$  is the absolute temperature,  $\rho$  is the density and  $\gamma$  is the dimensionless Grüneisen parameter. The Debye temperature  $\vartheta_D$  is directly related to the maximum frequency of vibration of the solid  $\nu_m$  as

$$\vartheta_D = \frac{h \nu_m}{k_B} \quad (2.3)$$

where  $h$  is the Planck constant ( $= 6.626 \times 10^{-34} \text{ J s}$ ) and  $k_B$  is the Boltzmann constant ( $= 1.381 \times 10^{-23} \text{ J K}^{-1}$ ). For silicate minerals, Horai and Simmons (1970) found an empirical relation between thermal conductivity and Debye temperature

$$\vartheta_D = 61.2 k_l + 385 \quad (2.4)$$

with  $k_l$  in  $\text{W m}^{-1} \text{K}^{-1}$  and  $\vartheta_D$  in kelvin. The Grüneisen parameter is weakly dependent on pressure and temperature (for most minerals it varies between 1.0 and 1.5) and expresses the ratio between thermal pressure and thermal energy per unit volume. It is defined as

$$\gamma = \frac{\alpha K_S}{\rho c_p} = \frac{\alpha K_T}{\rho c_v} \quad (2.5)$$

where  $c_p$  and  $c_v$  are the specific heats at constant pressure  $p$  and volume  $V$ ,  $K_S$  and  $K_T$  are bulk moduli at constant entropy  $S$  and temperature  $T$ , and  $\alpha$  is the thermal expansion coefficient.

In most rocks,  $k_l$  ranges from 1 to 7 W m<sup>-1</sup> K<sup>-1</sup>, with a few notable exceptions. Experiments confirm the inverse proportionality between  $k_l$  and  $T$ , and show for temperatures up to about 700 °C the validity of the empirical relation (Schatz and Simmons 1972; Balling 1976)

$$k_l = \frac{1}{a + b T} \quad (2.6)$$

where  $T$  is in °C,  $a = 0.33$  m K W<sup>-1</sup> and  $b = 0.33 \times 10^{-3}$  m W<sup>-1</sup> for the upper crust,  $a = 0.42$  m K W<sup>-1</sup> and  $b = 0.29 \times 10^{-3}$  m W<sup>-1</sup> for the lower crust. Thermal conductivity decreases from 3.0 W m<sup>-1</sup> K<sup>-1</sup> at the surface to about 2.0 W m<sup>-1</sup> K<sup>-1</sup> at 400 °C, and then decreases only very slightly at higher temperatures. In the lithospheric mantle,  $k_l$  is 2.0–2.5 W m<sup>-1</sup> K<sup>-1</sup>.

The lower crust and mantle temperatures are so high that the contribution of thermal radiation to conductivity must also be considered. At great depth, the heat transport through thermal radiation becomes important, and depends on the mineral opacity  $\varepsilon$  given by

$$\varepsilon = \frac{\ln(I_0/I)}{x} \quad (2.7)$$

where  $I_0$  is the intensity of the incident radiation and  $I$  the intensity of the radiation transmitted by a medium of thickness  $x$ . If opacity is independent from wavelength, the radiative conductivity  $k_r$  is defined by (Clark 1957)

$$k_r = \frac{16 n^2 \sigma T^3}{3 \varepsilon} \quad (2.8)$$

where  $n$  is the refractive index and  $\sigma$  the Stefan-Boltzmann constant ( $= 5.6705 \times 10^{-8}$  W m<sup>-2</sup> K<sup>-4</sup>); with  $n = 1.74$ , a typical value of ferromagnesian silicates, we have

$$k_r = 9.2 \times 10^{-7} \frac{T^3}{\varepsilon} \quad (2.9)$$

If  $\varepsilon$  were a constant,  $k_r$  would increase rapidly with temperature and would then be the dominant mechanism of heat transport. The radiative contribution has been measured on very few minerals. For olivine, by far the best studied, the experimental estimates are highly variable. According to Hasterok (2010), the radiative contribute is negligible at  $T < 600$  K and in the lithospheric mantle it can be described by

$$k_r = 0.56 \left[ 1 + \operatorname{erf} \left( \frac{T - 1150}{370} \right) \right] \quad (2.10)$$

with  $T$  in kelvin. Equation (2.10) gives values that significantly differ from previous estimates (Schatz and Simmons 1972; Hofmeister 2005; Hasterok and Chapman 2011). At temperature 1600 K,  $k_r$  is  $1.1 \text{ W m}^{-1} \text{ K}^{-1}$ .

Finally, we must take account of the effect of pressure on thermal conductivity. By excluding the sedimentary rocks with large porosity (see Sect. 2.4 for the effect on  $k$ ), the correction on  $k$  for igneous and metamorphic rocks at a pressure up to 100 MPa is positive (on average about 10 %). Under a higher pressure, there is a slight increase of  $k$ , on average by  $0.002 \text{ W m}^{-1} \text{ K}^{-1}$  per 100 MPa, due to the crystal lattice deformation up to the elastic limit (Schloessin and Dvořák 1972).

Another physical property that influences the rate at which heat dissipates through the material is the thermal diffusivity  $\kappa$ , which is defined as

$$\kappa = \frac{k}{\rho c} \quad (2.11)$$

where  $\rho$  is the density and  $c$  the specific heat. For most minerals and rocks,  $\kappa$  is of the order of  $10^{-6} \text{ m}^2 \text{ s}^{-1}$ . Diffusivity values of bituminous coal and rock salt are  $0.2 \times 10^{-6} \text{ m}^2 \text{ s}^{-1}$  and  $3 \times 10^{-6} \text{ m}^2 \text{ s}^{-1}$ , respectively. Grough (1979) derived a diffusivity of  $0.33 \times 10^{-6} \text{ m}^2 \text{ s}^{-1}$  for the upper mantle. For nonporous rocks,  $c$  ranges from about 0.7 to 1.1  $\text{kJ kg}^{-1} \text{ K}^{-1}$  and, at constant pressure, it is given by

$$c_p = 0.75(1 + 6.14 \times 10^{-4} T - 1.928 \times 10^4 T^{-2}) \quad (2.12)$$

where  $T$  is the absolute temperature. In case of saturated porous rocks,  $c$  can be calculated as a weighted average of the matrix and of the pore-filling fluid specific heat. The water specific heat is  $4.2 \text{ kJ kg}^{-1} \text{ K}^{-1}$  at room temperature and pressure, and it doubles at  $350^\circ \text{C}$  and 20 MPa. Under high pressure and temperature, the specific heat at constant volume,  $c_v$ , is related to  $c_p$  as

$$c_p/c_v = 1 + \alpha \gamma T \quad (2.13)$$

in which  $T$  is the absolute temperature and  $\gamma$  the Grüneisen parameter.

The ratio between thermal conductivity and the square root of thermal diffusivity defines the thermal inertia

$$\frac{k}{\sqrt{\kappa}} = \sqrt{k \rho c_v} \quad (2.14)$$

which is a measure of the rock responsiveness to temperature variations. If  $k = 2.3 \text{ W m}^{-1} \text{ K}^{-1}$  and  $\kappa = 0.8 \times 10^{-6} \text{ m}^2 \text{ s}^{-1}$ , we may determine a thermal inertial of  $2.6 \text{ kJ m}^{-2} \text{ K}^{-1} \text{ s}^{-1/2}$ . The higher specific heat the higher thermal inertia. If temperature variations occur with a characteristic thermal time  $\tau$ , they will propagate to a distance of the order of  $(\kappa \tau)^{1/2}$ . Similarly, a lapse of time  $l^2/\kappa$  is required for temperature changes to propagate to a distance  $l$ .

**Table 2.1** Naturally occurring, long-lived isotopes

Isotope	Abundance (wt%)	Decay mechanism	Half-life (years)	Final daughter product	Heat generation ( $\mu\text{W kg}^{-1}$ )
$^{238}\text{U}$	99.28	$8\alpha+6\beta^-$ $5.4 \cdot 10^{-5} \%$ fission	$4.47 \times 10^9$	$^{206}\text{Pb}$	91.7
$^{235}\text{U}$	0.71	$7\alpha+4\beta^-$	$7.04 \times 10^8$	$^{207}\text{Pb}$	575.0
$^{232}\text{Th}$	100	$6\alpha+4\beta^-$	$1.40 \times 10^{10}$	$^{208}\text{Pb}$	25.6
$^{40}\text{K}$	0.0118	$89.3 \%$ $\beta^-$ $10.7 \%$ $K$ $0.001 \%$ $\beta^+$	$1.25 \times 10^9$	$^{40}\text{Ca}$ $^{40}\text{Ar}$ $^{40}\text{Ar}$	30.0

Half-life =  $\ln 2 / \text{decay constant}$ .  $^{238}\text{U}$  and  $^{235}\text{U}$  abundances do not add to 100 % because  $^{234}\text{U}$  occurs in the decay series of  $^{238}\text{U}$ . Short-lived thorium isotopes,  $^{227}\text{Th}$ ,  $^{228}\text{Th}$ ,  $^{231}\text{Th}$  and  $^{234}\text{Th}$ , also occur in the decay series of  $^{238}\text{U}$ ,  $^{235}\text{U}$  and  $^{232}\text{Th}$

### 2.1.2 Radiogenic Heat

On a geological time scale, more than 98 % of the heat now being produced in rocks is yielded by the radioactive decay of  $^{238}\text{U}$ ,  $^{232}\text{Th}$  and  $^{40}\text{K}$ . These radioelements have half-lives which can be compared to the age of the Earth and are still sufficiently abundant to be an important source of heat. Their abundance, half-lives and energy release are given in Table 2.1.

The nuclei of these radioactive elements are unstable, i.e. they transform into other elements, typically by emitting (sometimes by absorbing) particles. This process, known as radioactive decay, generally results in the emission of alpha or beta particles from the nucleus. It is often also accompanied by the emission of gamma rays of different energies. In the natural uranium,  $^{238}\text{U}$  is the most abundant isotope (99.28 %). The other uranium isotopes are  $^{235}\text{U}$  (0.71 %), which has a shorter half-life than  $^{238}\text{U}$ , and  $^{234}\text{U}$ , which is of negligible importance (0.01 %).  $^{238}\text{U}$  undergoes a series of 14 radioactive decays (8 alpha and 6 beta emission) until it becomes  $^{206}\text{Pb}$ , a stable nonradioactive element.  $^{235}\text{U}$  decays instead through eleven steps (7 alpha and 4 beta emission) and its final product is  $^{207}\text{Pb}$ . Natural thorium is primarily formed by  $^{232}\text{Th}$ . All the decay products of  $^{232}\text{Th}$  have a comparatively short half-life and each nucleus decays through ten steps (6 alpha and 4 beta emission) to reach the final state as the stable isotope  $^{208}\text{Pb}$ .  $^{40}\text{K}$  is only 0.0118 % of the potassium found in nature. It presents a single-step decay, either transforming in  $^{40}\text{Ca}$  (by beta-emission) or  $^{40}\text{Ar}$  (by electron capture). The electron capture accounts for only the 10.7 % of decay events, but it produces the 1.46 MeV gamma-ray emission that is used for measuring the level of activity.

The energy radiated during the decay process is converted into heat by absorption. The radiogenic heat,  $A$ , can be calculated from the concentration  $c$  of uranium, thorium and potassium as

$$A = \rho \sum P A_s c \quad (2.15)$$

where  $\rho$  is the rock density,  $P$  the abundance and  $A_s$  the rate of heat generation per kilogram of isotope. By using the parameters of Table 2.1, (2.15) becomes (Chiozzi et al. 2002)

$$A = \rho (9.51 c_U + 2.56 c_{Th} + 3.50 c_K) 10^{-5} \quad (2.16)$$

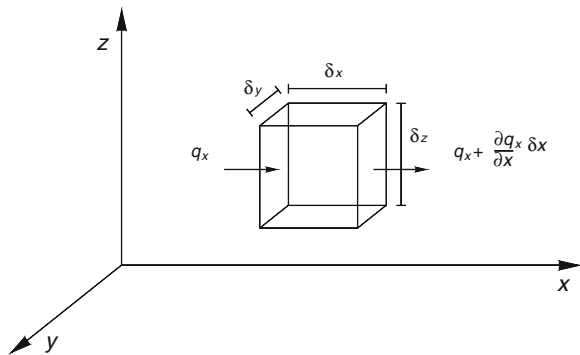
where  $A$  is in  $\mu \text{ W m}^{-3}$ ,  $\rho$  in  $\text{kg m}^{-3}$ , the uranium and thorium concentrations ( $c_U$  and  $c_{Th}$ ) in ppm (or  $\text{mg kg}^{-1}$ ) and potassium ( $c_K$ ) in %.

In general, uranium and thorium occur as trace elements, while potassium possibly as a mineralizer in all igneous, metamorphic and sedimentary rocks. Uranium and thorium are enclosed in the crystal lattice of minerals, in inclusions or ionic exchange positions incorporated or built into the mineral structure, and their amount increases with the silica concentration. The soluble part of these lithophile elements, absorbed at the surface of the crystal or found in pore spaces, becomes mobile as soon as water migrates through the rocks. Such a redistribution, especially of uranium, takes place not only during weathering, but also within the crust during magma cooling and in metamorphic processes. Metamorphism may even lead to redistribution of the less soluble part, enclosed in the crystal lattice.

## 2.2 Heat Conduction Equation

In the previous section, we saw that Fourier's law correlates the heat-flow density with the temperature gradient. By assuming appropriate boundary and initial conditions, this law can be used to determine the temperature distribution in solids, but only if heat is transferred through conduction. The heat-conduction equation can be obtained by considering a small element of volume  $\delta V$  of parallelepiped shape, with edges  $\delta x$ ,  $\delta y$ ,  $\delta z$  parallel to the coordinate axes (Fig. 2.1). If the amount of heat entering the volume element is smaller than the heat flowing out, in the  $x$  axis direction we have

**Fig. 2.1** Heat-flow density  $q_x$  in a small volume  $\delta V (= \delta x \delta y \delta z)$  in the direction of axis  $x$



$$\left( q_x + \frac{\partial q_x}{\partial x} \delta x \right) \delta y \delta z - q_x \delta y \delta z = \frac{\partial q_x}{\partial x} \delta V$$

Similar expressions are obtained for the other two directions, and the amount of heat removed from the volume element is

$$\left( \frac{\partial q_x}{\partial x} + \frac{\partial q_y}{\partial y} + \frac{\partial q_z}{\partial z} \right) \delta V \quad (2.17)$$

By indicating with  $A$  the heat production rate per unit of mass (for the lithosphere it correspond to the radiogenic heat) and with  $\partial Q / \partial t$  the heat change within  $\delta V$ , we can write

$$\left( \frac{\partial q_x}{\partial x} + \frac{\partial q_y}{\partial y} + \frac{\partial q_z}{\partial z} \right) \delta V = - \frac{\partial Q}{\partial t} + A \delta V \quad (2.18)$$

where the minus sign means that the heat loss, greater than the heat internally produced, causes a decrease of heat content in the element. As the variation of heat content with time  $t$  is related to the temperature variation as

$$\frac{\partial Q}{\partial t} = c \rho_p \frac{\partial T}{\partial t} \delta V \quad (2.19)$$

where  $\rho$  and  $c$  are the density and the specific heat at constant pressure, (2.18) becomes

$$\left[ \frac{\partial(-k_x \frac{\partial T}{\partial x})}{\partial x} + \frac{\partial(-k_y \frac{\partial T}{\partial y})}{\partial y} + \frac{\partial(-k_z \frac{\partial T}{\partial z})}{\partial z} \right] \delta V = -c \rho_p \frac{\partial T}{\partial t} \delta V + A \delta V$$

Thus, by dividing by  $\delta V$  and by assuming that thermal conductivity  $k$  is constant in the three directions and independent from temperature and pressure, for a homogeneous isotropic solid we have

$$k \nabla^2 T = c \rho_p \frac{\partial T}{\partial t} - A \quad (2.20)$$

For steady state conditions ( $\partial T / \partial t = 0$ ), from (2.20) it is possible to obtain Poisson's equation

$$k \nabla^2 T = -A \quad (2.21)$$

which in the absence of internal heat production ( $A = 0$ ) is reduced to Laplace's equation

$$\nabla^2 T = 0 \quad (2.22)$$

In the case of transient regime and negligible heat production instead, the Fourier equation is obtained

$$\nabla^2 T = \frac{1}{\kappa} \frac{\partial T}{\partial t} \quad (2.23)$$

The assumption of uniform conductivity is only an approximation, and in some cases it is necessary to keep  $k$  in the differential operator. The general equation of heat conduction, which gives the temperature within a heterogeneous solid, is then given by

$$\rho c_p \frac{\partial T}{\partial t} = \nabla k \nabla T + k \nabla^2 T + A(x, y, z, t) \quad (2.24)$$

which for a steady-state regime becomes

$$\nabla k \nabla T + k \nabla^2 T + A(x, y, z) = 0 \quad (2.25)$$

By using the vector identity

$$\nabla k = \left( \frac{dk}{dT} \right) \nabla T$$

equation (2.25) can be modified as

$$\frac{dk}{dT} (\nabla T)^2 + k \nabla^2 T + A(x, y, z) = 0 \quad (2.26)$$

For a semi-infinite half-space defined by  $z > 0$ , the solution of (2.26) with  $k = k_0/(1 + bT)$  and  $A = A_0 \exp(-z/d)$  is (Pasquale 1987)

$$T(z) = \frac{1}{b} \exp \left\{ \ln(1 + b T_0) + \frac{q_0 b}{k_0} z - \frac{A_0 b}{k_0} \left[ d \exp \left( -\frac{z}{d} \right) + z - d \right] \right\} - \frac{1}{b} \quad (2.27)$$

where  $k_0$  is thermal conductivity at room temperature,  $b$  and  $d$  are constants,  $T_0$ ,  $q_0$  and  $A_0$  are temperature, heat-flow density and heat production at depth  $z = 0$  (for  $b \rightarrow 0$ ,  $k$  is constant; for  $d \rightarrow \infty$ ,  $A$  is constant). For a plane-parallel multilayered model, with  $A_i$  and  $A_{i+1}$  the heat production at  $Z_i$  (upper) and  $Z_{i+1}$  (lower) depth of the  $i$ th layer, the temperature is given by

$$T(z) = \frac{1}{b_i} \exp \left\{ \ln(1 + b_i T_i) + \frac{q_i b_i (z - z_i)}{k_i} - \frac{A_i b_i d_i}{k_i} \left[ d_i \exp \frac{(z_i - z)}{d_i} + z - z_i - d_i \right] \right\} - \frac{1}{b_i} \quad (2.28)$$

where,  $b_i$  and  $k_i$  are the parameters (as defined above) of the layer,  $d_i = (z_{i+1} - z_i)/\ln(A_i/A_{i+1})$ ,  $q_i = q_{i+1} + A_i d_i \{1 - \exp[(z_i - z_{i+1})/d_i]\}$ ,  $T_i$  and  $q_i$  are, respectively, the temperature and heat-flow density at the depth  $z_i$ .



## 2.3 Thermal Conductivity Measurements

Methods for measuring thermal conductivity of soil and rocks may be classified into two categories: steady-state and transient. They both may give absolute or relative values, compared to standards, but in practice the steady-state methods are used in the comparative mode, whereas the transient methods in the absolute mode. Normally, transient methods give thermal diffusivity, however, under certain experimental conditions, they can measure directly thermal conductivity (see e.g. Tye 1969; Parrott and Stuckes 1975; Beck 1988, for a review).

Steady-state measurements on rocks are usually made by means of the divided-bar method, first described by Benfield (1939) and Bullard (1939). There are various modifications to this method, depending on the temperature and pressure needed as well as the rock specimen size (Birch 1950; Beck and Beck 1958; Sass et al. 1971; Blackwell and Spafford 1987). The rock specimen is placed between two blocks of known thermal conductivity. The setup is usually vertical, with the specimen between the hot block at the top and the cold block at the bottom; the heat transfers downwards preventing any convection within the specimen. Measurements are taken when a steady heat flow occurs along the bar.

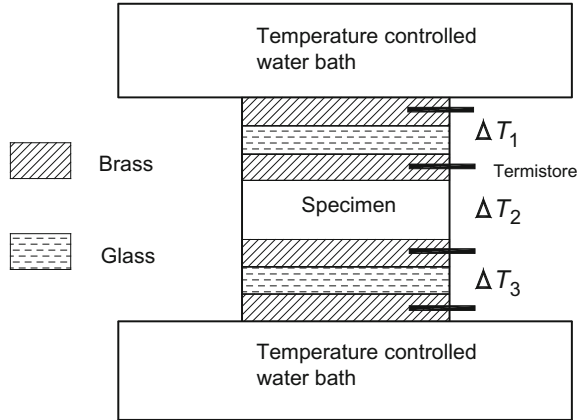
The most commonly used method for soft rocks is the needle probe, first described by De Vries and Peck (1958) and Von Herzen and Maxwell (1959). It is a transient method based on the theory of an infinite line heat source, embedded within an infinite material. In this configuration, the thermal response is detected by a temperature sensor located on the heat source. For hard rocks, measurements under transient conditions are usually made by means of a plane or a circular heat source, with a temperature sensor at the center (Beardsmore and Cull 2001).

The development of new electronic tools for data acquisition allowed the improvement of some classical methods, such as the line source (see Pribnow and Sass 1995, for a review) and the pulsed line source (Lewis et al. 1993). A further implementation of electronic data acquisition is the scanning of rock specimen surfaces with a focused, mobile and continuously operated, constant heat source, in combination with a temperature sensor (Popov 1983; Popov et al. 1999). Pasquale (1983) revised a method by Joffe and Joffe (1958) which was designed for determining the thermal conductivity of semiconductors, making it suitable for routine measurements on consolidated rocks. A synthesis of some classical methods is presented in the following sections.

### 2.3.1 Divided Bar

The divided bar is a steady-state method with an accuracy of 2 % (Jessop 1990). It uses a comparative technique in which the temperature drop across a disk of rock

**Fig. 2.2** Scheme of the divided bar method



specimen (or of a cylindrical cell containing water-saturated material) is compared with the temperature drop across two glass disks of known thermal conductivity (Fig. 2.2). Glass is chosen as the reference material since its thermal resistance is of the same magnitude as that of the specimen. Since these glass disks cannot be adapted to allow for the inclusion of temperature sensors, brass disks are inserted on both sides of each glass disk. The ends of the bar are kept at constant temperature by means of a thermostatic bath. The top bath is held about five degrees above room temperature and the bottom bath is five degrees below room temperature.

From each trial, four equilibrium temperature readings are performed. The relationship for thermal conductivity is based on the principle that the temperature drop is proportional to thermal resistance. The basic equation is

$$h_g \frac{\Delta T_2}{\Delta T_1 + \Delta T_3} = h_s \frac{k_g}{k_s} + R k_g \quad (2.29)$$

where  $k_s$  and  $h_s$  are the thermal conductivity and thickness of the rock specimen,  $k_g$  and  $h_g$  are the thermal conductivity and total thickness of the two glass disks, and  $R$  is an estimate of the total thermal resistance associated with the components of the divided bar

$$R \approx R_2 - (R_1 + R_3) \frac{h_s k_g}{h_g k_s} \quad (2.30)$$

$R_1$ ,  $R_2$  and  $R_3$  are the thermal resistances of the first glass disk, of the rock specimen and of the second glass disk, respectively, and  $\Delta T_1$ ,  $\Delta T_2$ ,  $\Delta T_3$  are the temperature differences across these elements. These resistances include the various contacts involving the baths, glass disks, rock specimen and brass disks.

If the thermal conductivity of the glass is known, it will be possible to deduce the thermal conductivity of the rock specimen from the ratio  $k_g/k_s$ , obtained as the linear slope of  $h_g \Delta T_2 / (\Delta T_1 + \Delta T_3)$  plotted against  $h_s$  for a set of specimens of the

same rock with varying thickness. The value of  $R$  can be inferred from the intercept. Generally, only one rock specimen is measured and a value of  $1.0 \times 10^{-4} \text{ K m}^2 \text{ W}^{-1}$  is assumed for  $R$ . A rock specimen of average conductivity and thickness (e.g. a 10 mm disk of sandstone) will give the bar an overall thermal resistance of about  $1.0 \times 10^{-2} \text{ K m}^2 \text{ W}^{-1}$ . Since the resistance  $R$  is only 1 % of the total thermal resistance across the bar, the approximation of  $R$  does not introduce a relevant error into the calculation.

### 2.3.2 Needle Probe

The needle probe method is based on the theory of an infinite line heat source embedded within an infinite material. The thermal response is detected by a temperature sensor located on the heat source. Typically, the needle probe has a diameter of 1–3 mm and is designed so as to package both the heat source and temperature sensor closely within the probe. A schematic diagram showing the components of a needle probe is shown in Fig. 2.3a.

For an infinite line source with constant power per unit length  $Q$ , the thermal conductivity  $k$  is given by (Carslaw and Jaeger 1986)

$$k = \frac{Q}{4\pi} \frac{\partial \ln t}{\partial T} \quad (2.31)$$

where  $t$  is time and  $T$  is temperature. If  $Q$  is known,  $k$  can be determined directly once  $\ln t$  versus  $T$  attains linearity. This is usually within 30 s, although a minimum of 200 s is generally required to establish unambiguous gradients. Experimental results show that the probe is able to measure thermal conductivity within a range of  $0.1\text{--}16 \text{ W m}^{-1} \text{ K}^{-1}$  with an uncertainty lower than 5 %.

This method provides a two-dimensional value for thermal conductivity for a plane perpendicular to the needle axis. The result obtained from a measurement of an anisotropic sample is related to the orientations of the principal axes of the thermal conductivity tensor ( $k_x$ ,  $k_y$  and  $k_z$ )

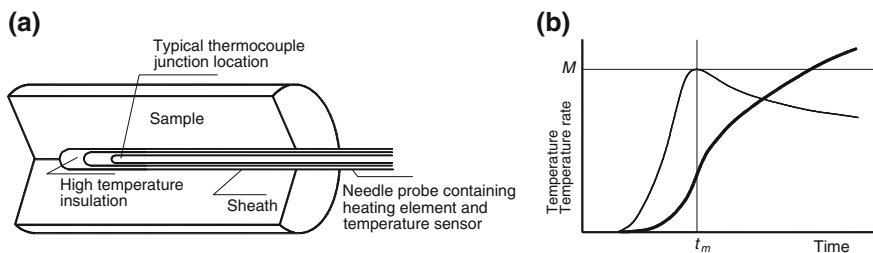


**Fig. 2.3** **a** Scheme of the needle probe method. **b** Temperature (thick line) and temperature rate (thin line) versus time at a distance  $r$  from the heat source

$$k = \sqrt{k_x k_y \cos^2 \gamma + k_x k_z \cos^2 \beta + k_y k_z \cos^2 \alpha} \quad (2.32)$$

where  $\alpha$ ,  $\beta$  and  $\gamma$  are angles between the line-source axis and the principal axes of thermal conductivity  $x$ ,  $y$  and  $z$ , respectively (Popov et al. 1999). Due to layering, many sedimentary rocks are transversally isotropic ( $k_x = k_y$ ). The thermal conductivity tensor can then be defined by two principal components that are perpendicular ( $k_{per} = k_z$ ) and parallel ( $k_{par} = k_x = k_y$ ) to layering. When the needle is parallel to the bedding ( $\alpha = 0$  and  $\beta = \gamma = 90^\circ$ ), (2.32) can be simplified into

$$k = \sqrt{k_{par} k_{per}} \quad (2.33)$$

i.e. the measured thermal conductivity is the geometric mean of the parallel and perpendicular components.

As the temperature gradient may induce convection within rock specimen with large porosity, the maximum gradient technique has been developed (Cull 1975). The rate of the temperature increase at a distance  $r$  from the line source can be expressed as

$$\frac{\partial T}{\partial t} = \frac{Q}{4 \pi k t} \exp\left(-\frac{r^2}{4 \kappa t}\right) \quad (2.34)$$

where  $\kappa$  is the thermal diffusivity. At time  $t_m$ , this equation has a maximum value of  $M$  (Fig. 2.3b). For  $\partial^2 T / \partial t^2 = 0$  we obtain  $\kappa = r^2 / (4 t_m)$ , which substituted back into (2.34) gives

$$k = 0.0293 \, Q / (M \, t_m) \quad (2.35)$$

Since  $M$  and  $t_m$  can be determined and  $Q$  is known, thermal conductivity can thus be calculated.

This technique is put into practice using a dual-needle probe with one needle housing the heating wire and the other the temperature sensor at a distance of about 3 mm. Nevertheless, the dual-needle configuration may be unsuitable for measurements in coarse-grained material. For such rock specimen, measurements are better made with a circular heat source (ring) with a temperature sensor at the center. In this case, (2.35) becomes

$$k = 0.0771 \, Q / (M_1 \, t_{1m}) \quad (2.36)$$

where  $t_{1m} = r^2 / (6 \kappa)$  and  $M_1$  is the maximum value of the rate of temperature change at the center of the ring of radius  $r_1 (= 0.50 - 0.75 \text{ cm})$  expressed as (Somerton and Mossahebi 1967)

$$\frac{\partial T}{\partial t} = \frac{Q \, r}{4 (\pi \kappa t^3)^{1/2}} \exp\left(-\frac{r^2}{4 \kappa t}\right) \quad (2.37)$$

$Q$  is heat per unit length of wire per unit of time.

### 2.3.3 Transient Divided Bar

This method is somewhat similar to that developed by Joffe and Joffe (1958) to measure the thermal conductivity of poor conductors. A thermal stack is arranged, consisting of a cylindrical specimen of rock placed between two cylindrical blocks of copper of known thermal capacity (Fig. 2.4a). The upper block acts as a heat source and the lower block, more massive, as a heat sink. The heat flowing through the specimen is equal to the heat absorbed by the sink; in this way thermal conductivity can be found by measuring the changes in temperature at the source and sink.

The experiment begins when the stack of elements reaches the room temperature  $T_o$ . The lower block is then cooled by immersing it into a thermostatic bath whose temperature is 10–15 °C lower than  $T_o$ . The temperatures of the upper ( $T_u$ ) and lower ( $T_l$ ) blocks are recorded by using thermocouples placed as close as possible to the specimen. After a few minutes a uniform temperature gradient ( $T_u - T_l$ )/ $h$  is established (Fig. 2.4b).

On the base of the Fourier's law and calorimetric law, the amount of heat removed from the upper block, in a given time step  $\Delta t$ , is given by

$$C_u \Delta T_u = \frac{k' S}{h} \int_1^2 (T_u - T_l) dt = \frac{k' S}{h} (\bar{T}_u - \bar{T}_l) \Delta t$$

from which

$$k' = \frac{C_u \Delta T_u h}{S (\bar{T}_u - \bar{T}_l) \Delta t} \quad (2.38)$$

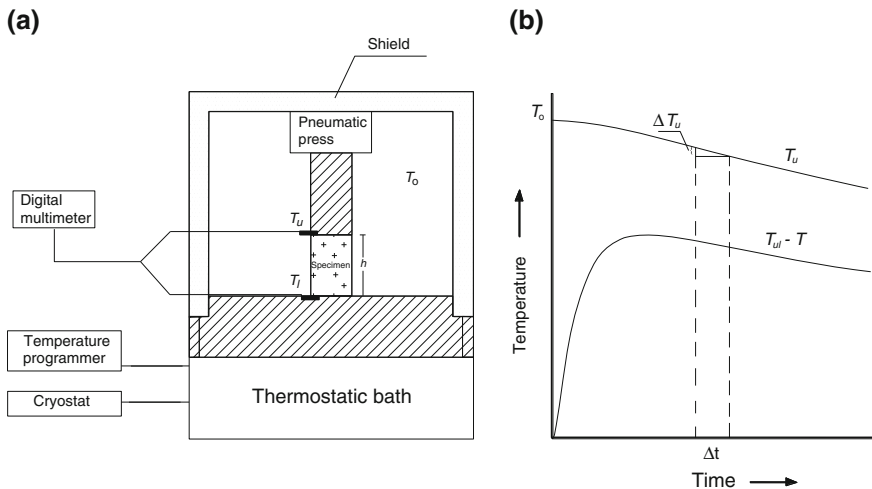


**Fig. 2.4** **a** Scheme of the transient divided bar method. **b**  $T_u$  and  $T_u - T_l$  curves recorded during the experiment

where

$k'$  is thermal conductivity of the rock specimen,

$C_u$  is the thermal capacity at constant pressure of the upper block,

$h$  is the height of the specimen,

$S$  is the cross-sectional area of the specimen,

$\Delta T_u$  is the variation of  $T_u$  during time step  $\Delta t = t_2 - t_1$ ,

$(\bar{T}_u - \bar{T}_l)$  is the difference between the average values of  $T_u$  and  $T_l$  during  $\Delta t$ .

Theoretical analysis of this method (Kaganov 1958; Swann 1959; Drabble and Goldsmith 1961) showed that two additional thermal processes can take place while measuring. The first has to do with the heat coming from the rock specimen, the second with the heat transferred from the surrounding environment to the upper block. Thus, two corrections must be introduced.

The heat flowing from the specimen is taken into account by considering the quantity  $(C_u + C_s/3)$  instead of  $C_u$ , where  $C_s$  is the specimen thermal capacity. In order to estimate the correction for the heat transmitted from the environment, it is necessary to operate under steady-state conditions, when the temperatures  $T_u$  and  $T_l$  are constant, i.e. about 2 h after the experiment begins. The upper block absorbs heat from the environment, whose temperature  $T_o$  is kept constant during the measurement. Under steady-state conditions, the heat  $Q_s$  transmitted from the upper block, at constant temperature  $T_{us}$ , to the lower block, at constant temperature  $T_{ls}$ , will be equal to

$$Q_s = F (T_o - T_{us}) = \frac{k' (T_{us} - T_{ls}) S \Delta t}{h} \quad (2.39)$$

from which it is possible to calculate the quantity  $F$ . During the experiment, the relation

$$Q = F (T_o - \bar{T}_u) \quad (2.40)$$

holds, which for each  $\bar{T}_u$  allows the calculation of the amount of heat coming from the environment. By taking into account the foregoing corrections, the effective thermal conductivity  $k$  is then given by

$$k = \frac{[(C_u + C_s/3) \Delta T_u + F (T_o - \bar{T}_u)] h}{(\bar{T}_u - \bar{T}_l) S \Delta t} \quad (2.41)$$

A main source of error on thermal conductivity determinations with this method lies in the difficulty of eliminating the thermal contact resistance between the blocks and the rock specimen. Particular care should be taken in preparing the specimen base surfaces, making them flat to within 0.1 mm (no wedge shape), smoothed and mutually parallel to within 0.03 mm throughout (no dome or concavities). A film of silicone paste is smeared on the contact surfaces and a light pressure is exerted on the upper block in order to improve the contact. The thermal resistance of the silicon film about 0.01 mm-thick is equivalent to a rock sheet of a

few hundredths of a millimeter. Such a resistance, for an adopted standard height of the specimen (about 2 cm) is less than 2 % of the total thermal resistance of the rock specimen.

If the lateral heat loss is neglected, the time range for which the temperature data should be reliable and a reasonable accuracy achieved falls within the limits of the following inequality (Kaganov 1958)

$$\frac{\ln 2 h^2}{\pi^2 \kappa} \ll t \leq \frac{C_u h^2}{C_s \kappa} \quad (2.42)$$

where  $\kappa$  is the rock thermal diffusivity. The order of magnitude of  $t$  is of a few minutes. For  $k$  ranging from 1 to 10 W m<sup>-1</sup> K<sup>-1</sup>, the experimental error is less than 5 % and the reproducibility of about 3 %. This method is unaffected by thermal convection within the specimen as, similarly to the divided bar method, the lower block is kept at a lower temperature. The upper block and the specimen are housed in order to minimize air current effects on the environment temperature. The best performances are obtained when the specimen radius is equal to that of upper block. The specimen height has an effect only if the radius is smaller than the optimal one.

### 2.3.4 Data Compilation

Thermal conductivity of a variety of water-saturated isotropic sedimentary rocks obtained with the transient divided bar method is given in Table 2.2. In addition to thermal conductivity, porosity and density are listed. Rock porosity is calculated as the ratio of the difference of grain and bulk densities to the grain density. Mass change between dehydrated and water-saturated conditions is accounted for by the influx of water into the pore spaces (this procedure yielded a direct measurement of porosity). The solid volume of argillaceous and evaporitic rocks is inferred with a helium pycnometer. Closed interstices, i.e. the pores that are not connected to the rock surface, are included in the measured volume.

The analyzed rocks were recovered from petroleum exploration wells up to a depth of about seven kilometer and form a broad collection of lithologies. Most of them are clastic and macroscopically isotropic. Clastic rocks consist of framework silicates and carbonate grains in an argillaceous matrix or calcareous cement. Most rocks are marls and silty marls of marine origin, formed by calcium carbonate mud containing a variable amount of clays. The sampled argillaceous sandstones are lithic and feldspatic arenites, primarily composed by cemented sandy sediment, in many cases with a predominance of sand-sized rock fragments and quartz. Chemical/biochemical sediments include carbonatic, evaporitic and siliceous rocks. Evaporitic rocks (anhydrite and gypsum) are fine grained. In anhydrites, gypsum and calcite minerals are also present. Siliceous rocks are represented by radiolarites.

**Table 2.2** Thermal conductivity  $k$  (water-saturated), porosity and density of isotropic sedimentary rocks (Pasquale et al. 2011)

Rock	Lithotype	$n$	$k$ ( $\text{W m}^{-1} \text{K}^{-1}$ )		Porosity (%)		Density ( $\text{kg m}^{-3}$ )	
			Range	Mean	Range	Mean	Range	Mean
Clastic	Marl	19	2.15–3.08	2.77 (0.23)	6.0–37.0	15.1 (8.4)	1787–2530	2278 (240)
	Silty marl	18	2.85–3.66	3.16 (0.26)	2.0–20.0	12.8 (5.5)	2150–2670	2359 (156)
	Calcareous marl	6	1.99–2.37	2.17 (0.13)	22.0–35.0	30.8 (5.0)	1693–2008	1801 (123)
	Argillaceous limestone	3	3.58–3.63	3.60 (0.03)	7.5–12.0	9.3 (2.4)	2477–2588	2520 (80)
	Argillaceous sandstone	6	2.60–3.40	3.00 (0.29)	8.0–25.0	15.1 (6.2)	1990–2560	2330 (222)
	Calcarenite	3	2.18–2.50	2.34 (0.16)	25.0–32.0	29.0 (3.6)	1834–1997	1917 (82)
Chemical- biochemical	Mudstone	5	3.04–3.48	3.30 (0.16)	0.5–6.0	2.7 (2.1)	2550–2695	2630 (59)
	Wackestone	5	3.10–3.20	3.16 (0.04)	3.0–10.0	6.0 (3.0)	2500–2670	2590 (75)
	Packstone	4	3.00–3.45	3.23 (0.18)	3.0–6.0	4.3 (1.3)	2550–2655	2620 (59)
	Grainstone	5	2.95–3.36	3.12 (0.16)	6.5–12.0	8.8 (2.5)	2400–2540	2480 (73)
	Dolostone	5	4.25–5.45	4.60 (0.49)	1.5–7.5	3.8 (2.4)	2630–2800	2735 (73)
	Radiolarite	4	3.16–3.46	3.37 (0.14)	0.5–5.5	2.4 (2.2)	2550–2650	2600 (48)
Evaporitic	Anhydrite	5	3.15–3.65	3.39 (0.22)	0.5–5.0	2.7 (1.8)	2680–2780	2730 (52)
	Gypsum	5	1.40–1.64	1.54 (0.09)	0.5–7.0	2.4 (2.6)	2260–2400	2350 (61)

In brackets, the standard deviation.  $n$  is number of specimens



**Table 2.3** Thermal conductivity  $k$  and density of igneous and metamorphic rocks (Pasquale et al. 1988)

Lithotype	$n$	$k$ (W m <sup>-1</sup> K <sup>-1</sup> )		Density (kg m <sup>-3</sup> )	
		Range	Mean	Range	Mean
Granite	22	2.44–3.49	2.88 (0.26)	2590–2760	2620 (20)
Granodiorite	16	2.24–3.03	2.52 (0.24)	2640–2820	2690 (40)
Tonalite	10	2.06–2.25	2.16 (0.07)	2700–2760	2720 (20)
Syenite	3	2.19–2.34	2.25 (0.08)	2680–2750	2720 (40)
Diorite	14	1.73–2.07	1.89 (0.11)	2740–2940	2840 (60)
Gabbro	12	1.65–2.29	1.94 (0.19)	2800–3060	2940 (80)
Dacite	4	3.56–3.91	3.73 (0.18)	2500–2690	2610 (102)
Anorthosite	4	1.67–1.83	1.76 (0.07)	2660–2810	2730 (60)
Hornblende	5	2.57–2.79	2.71 (0.08)	3020–3180	3130 (70)
Lherzolite	11	3.31–4.00	3.70 (0.25)	3010–3210	3110 (50)
Harzburgite	3	3.52–3.66	3.60 (0.07)	3070–3110	3090 (20)
Dunite	3	4.04–4.16	4.11 (0.06)	3320–3360	3340 (20)

In brackets, the standard deviation  $n$  is number of specimens

The mean thermal conductivity ranges from 1.5 to 4.6 W m<sup>-1</sup> K<sup>-1</sup>, corresponding to gypsum and dolostone, respectively. Besides dolostones, larger values of conductivity characterize anhydrites, whereas lower conductivity is typical of calcareous marls. Carbonate rocks and argillaceous sandstones show intermediate values. Porosity varies from about 3 % (radiolarite, gypsum, mudstone and anhydrite) to 30 % (calcareous marl).

Table 2.3 shows thermal conductivity values measured on samples of igneous and metamorphic rocks, macroscopically homogeneous and isotropic. Plutonic rocks are mostly granitoid with a composition ranging from granitic to tonalitic; gabbro-dioritic rocks (syenites, anorthosites and hornblendites) are also listed. Ophiolitic rock are mainly peridotites of lherzolitic and harzburgitic type, more or less affected by serpentinization, and, to a smaller extent, of dunitic type, therefore containing almost exclusively olivine. Moreover, there are a few dacitic samples, recovered from deep borehole, belonging to intrasedimentary volcanic bodies. Due to the low porosity of crystalline rocks (mainly below 1.5 %), thermal conductivity is very close to that of rock matrix, and it ranges from 1.8 to 4.1 W m<sup>-1</sup> K<sup>-1</sup>.

Data presented in Tables 2.2 and 2.3 are of course additional to several earlier compilations (Birch 1942; Clark 1966; Desai et al. 1974; Kappelmeyer and Hänel 1974; Roy et al. 1981; Čermák and Rybach 1982; Robertson 1988; Zoth and Hänel 1988; Clauser and Huenges 1995). In general thermal conductivity values of igneous and metamorphic rocks are comparable for all datasets, because they depend mainly on mineral composition. For sedimentary rocks, instead thermal conductivity also depends on porosity. Within a particular lithotype, there may be a wide variation in porosity, which may consequently cause big differences in thermal properties. Thus, knowledge of sedimentary rock porosity is essential for an appropriate comparison of datasets.

## 2.4 Estimates of Thermal Properties

### 2.4.1 Mixing Models

Besides laboratory techniques, indirect approaches have been developed to estimate thermal conductivity and volumetric heat capacity of isotropic rocks (e.g. Schärli and Rybach 2001; Wang et al. 2006; Abdulagatova et al. 2009). Thermal properties can be inferred from information on volume fraction and conductivity of rock-forming minerals. This approach requires the modeling of the distribution of the various constituents. Literature values of thermal conductivity, density and specific heat of the main rock-forming minerals are summarized in Table 2.4. Thermal parameters for potassium feldspar, plagioclase and sheet silicates correspond to the most abundant minerals, i.e. microcline, oligoclase and the smectite-illite mineral group.

Provided that the mineral composition and physical properties of minerals and air are known, the volumetric heat capacity of a dry rock  $(\rho c)_r$  can be computed as the weighted average of the volumetric heat capacity of the matrix  $(\rho c)_m$  and of the air  $(\rho c)_a$  in the voids

$$(\rho c)_r = (1 - \phi)(\rho c)_m + \phi(\rho c)_a \quad (2.43)$$

where

$$(\rho c)_m = \sum_{j=1}^n v_j \rho_j c_j$$

$$\sum_{j=1}^n v_j = 1$$

**Table 2.4** Thermal conductivity, density and specific heat of rock-forming minerals, air and water at standard laboratory conditions

Material	Thermal conductivity (W m <sup>-1</sup> K <sup>-1</sup> )	Density (kg m <sup>-3</sup> )	Specific heat (J kg <sup>-1</sup> K <sup>-1</sup> )
Quartz- $\alpha$	7.69 <sup>a</sup>	2647 <sup>a</sup>	740 <sup>b</sup>
Quartz microcrystalline	3.71 <sup>a</sup>	2618 <sup>a</sup>	735 <sup>b</sup>
Plagioclase	1.97 <sup>a</sup>	2642 <sup>a</sup>	837 <sup>b</sup>
K-feldspar	2.40 <sup>a</sup>	2562 <sup>a</sup>	700 <sup>b</sup>
Calcite	3.59 <sup>a</sup>	2721 <sup>a</sup>	815 <sup>b</sup>
Dolomite	5.51 <sup>a</sup>	2857 <sup>a</sup>	870 <sup>b</sup>
Sheet silicates	1.88 <sup>c</sup>	2630 <sup>c</sup>	832 <sup>d</sup>
Anhydrite	4.76 <sup>a</sup>	2978 <sup>a</sup>	585 <sup>b</sup>
Gypsum	1.30 <sup>c</sup>	2320 <sup>b</sup>	1070 <sup>b</sup>
Air	0.026	1.225	1005
Water	0.60	1000	4186

<sup>a</sup> Horai (1971), <sup>b</sup> Waples and Waples (2004a), <sup>c</sup> Brigaud and Vasseur (1989), <sup>d</sup> Hadglu et al. (2007), <sup>e</sup> Clauser and Huenges (1995)

$\phi$  is porosity,  $v_j$ ,  $\rho_j$  and  $c_j$  are the volume fraction, density and specific heat of the  $j$ th mineral, respectively, and  $n$  is the number of mineral components.

Among the several models involving the application of mixing laws for a mineral aggregate, the model by Hashin and Shtrikman (1962), which was originally proposed to study the magnetic permeability of macroscopically homogeneous and isotropic materials, is currently the most used to calculate thermal conductivity. The matrix conductivity of the rock  $k_{mo}$  is given by

$$k_{mo} = \frac{(k_U + k_L)}{2} \quad (2.44)$$

where  $k_U$  is the conductivity upper bound defined as

$$k_U = k_{max} + \frac{A_{max}}{1 - a_{max} A_{max}} \quad (2.45)$$

$k_{max}$  is the maximum thermal conductivity of the mineral phases,  $a_{max} = (3 k_{max})^{-1}$  and

$$A_{max} = \sum_{j=1}^n \frac{v_j}{\frac{1}{(k_j - k_{max})} + a_{max}} \quad \text{for } k_j \neq k_{max} \quad (2.46)$$

where  $k_j$  is the thermal conductivity of the  $j$ th mineral, and  $v_j$  and  $n$  are as in (2.43). By replacing the minimum thermal conductivity of the mineral phases and the index 'max' with 'min' in (2.45) and (2.46), a similar expression can be obtained for the lower conductivity bound  $k_L$ .

In order to determine the bulk conductivity, it is necessary to take into account porosity. According to Zimmerman (1989), pores can be modeled as isolated spheroids and their shape is defined by the aspect ratio,  $a$ , i.e. the ratio of the length of the unequal axis to the length of one of the equal axes. Thus, pores have spherical, oblate and prolate shape for  $a = 1$ ,  $a < 1$  and  $a > 1$ , respectively. In extreme cases, i.e. when pores consist of thin cracks, spheroids assume a needle-like, tubular shape ( $a \rightarrow \infty$ ) or thin coin-like shape ( $a \rightarrow 0$ ). For an isotropic rock, an average orientation of the unequal axis of the spheroid with respect to the temperature gradient is considered. If the pores are randomly oriented and distributed spheroids, the computed thermal conductivity  $k_{HZ}$  is

$$k_{HZ} = k_{mo} \frac{[(1 - \phi) (1 - r) + r \beta \phi]}{[(1 - \phi) (1 - r) + \beta \phi]} \quad (2.47)$$

where  $k_{mo}$  is the matrix thermal conductivity of (2.44),  $\phi$  the porosity and  $r$  the ratio of thermal conductivity of the pore-filling water and the matrix thermal conductivity. The parameter  $\beta$  is given by

$$\beta = \frac{(1 - r)}{3} \left[ \frac{4}{2 + M(r - 1)} + \frac{1}{1 + (r - 1)(1 - M)} \right]$$

where for  $a < 1$

$$M = \frac{2\theta - \sin 2\theta}{2 \tan \theta \sin^2 \theta}$$

and for  $a > 1$

$$M = \frac{1}{\sin^2 \theta} - \frac{\cos^2 \theta}{2 \sin^3 \theta} \ln \left( \frac{1 + \sin \theta}{1 - \sin \theta} \right)$$

with  $\theta = \cos^{-1}(1/a)$ . For  $a = 1$ ,  $M = 3(1 - r)/(2 + r)$ .

Another technique to infer thermal conductivity is the geometric mixing model (see e.g. Jessop 1990)

$$k_G = \prod_{j=1}^n k_j^{v_j} \quad (2.48)$$

where symbols are as in (2.46). This method provides a less satisfactory estimate as the difference between computed and measured values is on average of  $\pm 5 - 10 \%$ .

### 2.4.2 In situ Thermal Properties

The assessment of thermal properties at depth is of paramount importance in geothermal studies. For sedimentary rocks, the problem can be approached with a technique based on mineral composition or, alternatively, lithostratigraphic data available from drilling reports (see Pasquale et al. 2008, 2011). The in situ thermal conductivity  $k_{in}$  can be obtained with the geometric mixing model

$$k_{in} = k_m^{(1-\phi)} k_w^\phi \quad (2.49)$$

where  $k_m$  and  $k_w$  are the matrix and water thermal conductivity, respectively. Porosity is assumed to decrease with depth  $z$  as

$$\phi = \phi_o e^{-bz} \quad (2.50)$$

where  $b$  is the compaction factor and  $\phi_o$  is the surface porosity. By expressing depth in kilometers, values adopted for  $\phi_o$  and  $b$  are  $0.180$  and  $0.396 \text{ km}^{-1}$  in carbonate rocks,  $0.298$  and  $0.461 \text{ km}^{-1}$  in marls and silty marls,  $0.284$  and  $0.216 \text{ km}^{-1}$  in sandstones and calcarenites, and  $0.293$  and  $0.379 \text{ km}^{-1}$  in shales and siltstones, respectively. Carbonate rocks, marls and sandstones are considered as isotropic, whereas in case of clay-rich lithologies (siltstones and shales) thermal anisotropy must be taken into account. In anisotropic rocks, the vertical matrix conductivity, which decreases with depth due to the orientation of the clay and mica platelets during burial, is estimated by using the relation

$$k_m = 2.899 - 0.251z \quad (2.51)$$

The water thermal conductivity  $k_w$  is assumed to change with temperature as suggested by Deming and Chapman (1988)

$$k_w = 0.5648 + 1.878 \times 10^{-3} T - 7.231 \times 10^{-6} T^2 \quad \text{for } T \leq 137^\circ\text{C} \quad (2.52)$$

$$k_w = 0.5648 + 1.878 \times 10^{-3} T - 7.231 \times 10^{-6} T^2 \quad \text{for } T \leq 137^\circ\text{C} \quad (2.53)$$

whereas the temperature dependence of the matrix conductivity is evaluated with the expression (Sekiguchi 1984)

$$k_m = 1.8418 + (k_o - 1.8418) \left( \frac{1}{0.002732 T + 0.7463} - 0.2485 \right) \quad (2.54)$$

where  $k_o$  is the matrix conductivity at  $20^\circ\text{C}$ . The total uncertainty in thermal conductivity, which takes into account the errors in the corrections for anisotropy, temperature and porosity, is 10 %.

Figure 2.5 shows as an example a profile of  $k_{in}$  modeled for two wells.  $k_{in}$  is calculated at the middle-point of 20 m intervals. In the uppermost kilometers, the compaction effect is larger than that due to the temperature and, for the same lithotype, this causes an increase of conductivity with depth. Both wells show that the maximum values of  $k_{in}$  occur in mudstones and sandstones. Horizons of silty shales are present at different depths and exhibit minima of conductivity. In these horizons, due to the presence of thermally anisotropic sheet silicates, conductivity is constant or decreases with depth.

The in situ volumetric heat capacity  $(\rho c)_{in}$  can be computed as the weighted average of the volumetric heat capacity of the matrix  $(\rho c)_m$  and the volumetric heat capacity of water  $(\rho c)_w$  in the voids

$$(\rho c)_{in} = (1 - \phi) (\rho c)_m + \phi (\rho c)_w \quad (2.55)$$

The specific heat of both water and matrix increases with temperature. Somerton (1992) proposed an expression for the specific heat of pure water as a function of temperature, which is proven valid in the 20–290  $^\circ\text{C}$  range

$$c_w = \frac{(4245 - 1.841 T) \times 10^3}{\rho_w} \quad (2.56)$$

where  $\rho_w$  is the density of liquid water, whose temperature dependence is

$$\rho_w = \frac{\rho_{w20}}{1 + (T - 20) \alpha_w} \quad (2.57)$$

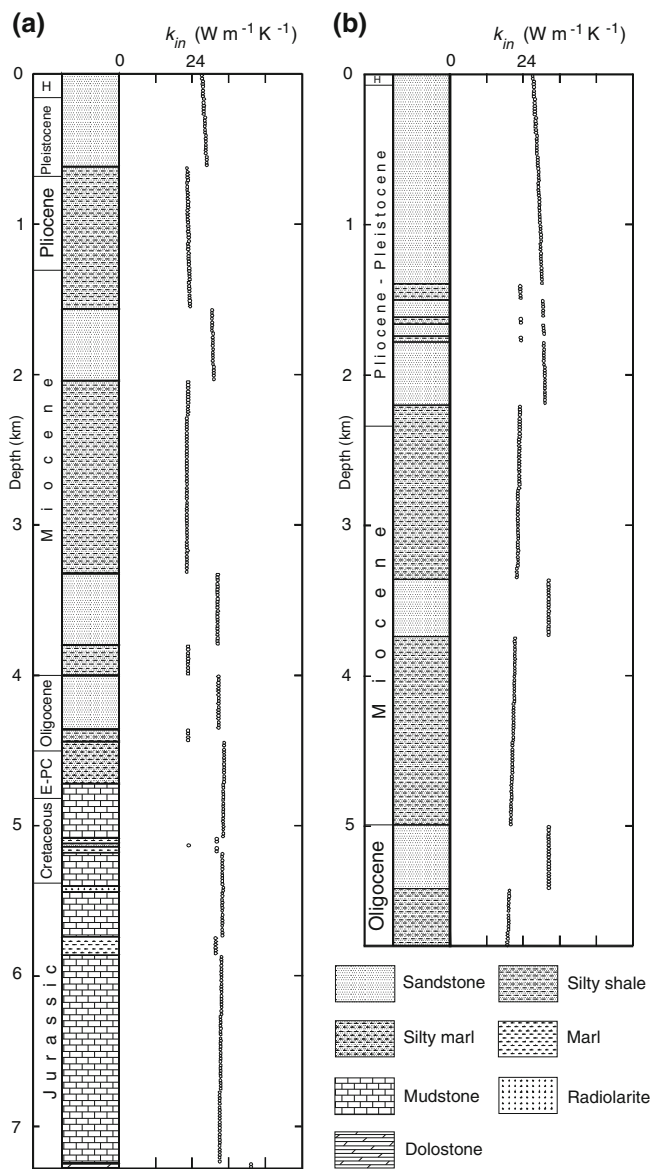


**Fig. 2.5** Vertical thermal conductivity as inferred from lithostratigraphic information at Belvedere (a) and Sali Vercellese (b) wells, Po Basin, Italy (after Pasquale et al. 2012). H = Holocene, E-PC = Eocene–Paleocene

with  $\rho_{w20}$  the water density at 20 °C, and  $\alpha_w$  the expansion coefficient of water given by

$$\alpha_w = 0.0002115 + 1.32 \times 10^{-6} T + 1.09 \times 10^{-8} T^2 \quad (2.58)$$

As long as the pressure is high enough to keep the water in a liquid phase, the volumetric heat capacity of water  $(\rho c)_w$ , under subsurface (high pressure) conditions, can be estimated with good accuracy from (2.56) to (2.58), without including pressure dependence (Somerton 1992; Waples and Waples 2004b).

Since the thermal expansion coefficient of rocks is very small (about  $10^{-5} \text{ K}^{-1}$ ), in a region of normal geothermal gradient, density can be considered as constant for a wide range of depths. Thus, the temperature dependence of the matrix volumetric heat capacity is controlled by the increase of the specific heat as a function of temperature. The temperature dependence of volumetric heat capacity for any mineral matrix can be computed with the equation (Hantschel and Kauerauf 2009)

$$(\rho c)_m = (\rho c)_{m20} (0.953 + 2.29 \times 10^{-3} T - 2.835 \times 10^{-6} T^2 + 1.191 \times 10^{-9} T^3) \quad (2.59)$$

where  $(\rho c)_{m20}$  is the volumetric heat capacity of the rock matrix at 20 °C.

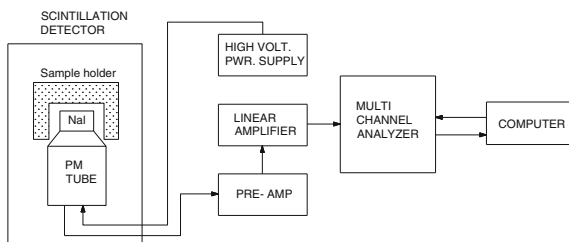
## 2.5 Determination of Heat-Producing Elements

Among the different analytical techniques used to determine the concentration of heat-producing elements (see e.g. Rybach 1988, for a brief review), gamma-ray spectrometry is the only one that allows the simultaneous assesement of U, Th and K. Although germanium semiconductor detectors are finding an increasing application in the determination of heat-producing elements, sodium iodide scintillation detectors offer fast and accurate results in ordinary crustal rocks. These detectors are versatile tools for a wide range of geophysical applications, including not only ground radiometric surveys for uranium, vehicle investigations for hydrocarbon and small airborne prospecting, but also laboratory data analysis and core logging services.

### 2.5.1 Laboratory Techniques

A typical scintillation spectrometer that uses a thallium-activated sodium iodide scintillation detector, coupled to a photomultiplier (PM) tube and a multi-channel (usually 256 or 1024) pulse-height analyzer for storage of the energy spectrum, is shown in Fig. 2.6. The analyzer is usually equipped with a spectrum stabilizer for

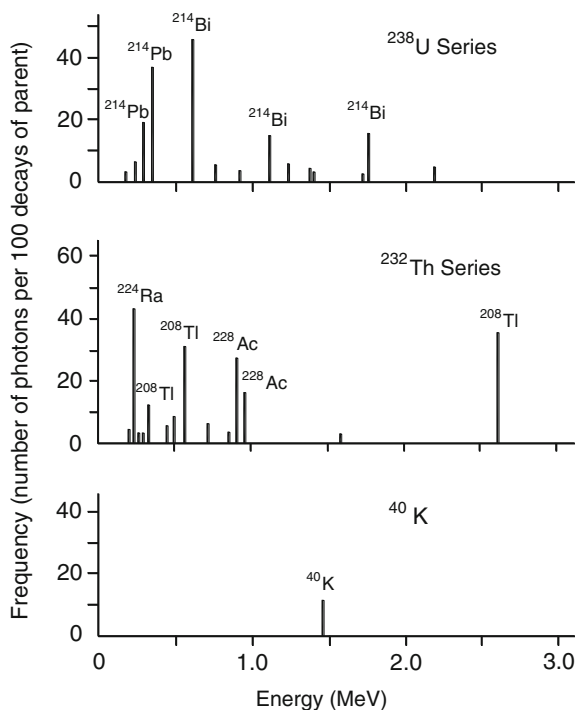
**Fig. 2.6** A block diagram of a typical system for gamma-ray spectrometry



automatic gain shift compensation. The detector is surrounded by a 5–10 cm thick lead shield, which reduces the amount of background gamma radiation. The sample preparation requires grinding the rock and encasing it in polyethylene Marinelli beakers. If a 500 ml beaker is adopted, the investigated rock samples approximately range in weight from 0.650 to 0.850 kg (Chiozzi et al. 2000a).

The gamma-ray energy spectrum emitted from a rock is the sum of the individual characteristic spectra of each radiogenic component (Fig. 2.7). The total signal can thus be analyzed to determine the amount of each element. The system is calibrated by means of three reference materials for K, U and Th activity (IAEA 1987). Usually, the method of the three energy windows described by Rybach (1971 and 1988) is adopted. Windows are set on the three characteristic energy

**Fig. 2.7** Principal gamma-rays (only energies >0.100 MeV) during the decay of  $^{238}\text{U}$  and  $^{232}\text{Th}$  series and  $^{40}\text{K}$ . Data from Lederer and Shirley (1978)





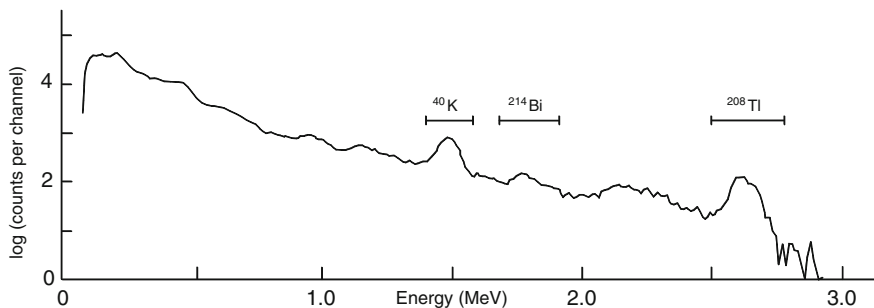


**Fig. 2.8** Gamma-ray spectrum obtained for a shoshonitic lava flow and energy windows utilized for data processing (Chiozzi et al. 2003). The counts in each energy channel are represented with a solid line

photo-peaks, i.e. at 1.46, 1.76 and 2.62 MeV, corresponding to  $^{40}\text{K}$ ,  $^{214}\text{Bi}$  ( $^{238}\text{U}$  series) and  $^{208}\text{Tl}$  ( $^{232}\text{Th}$  series), respectively (Fig. 2.8). The gamma-ray count rate for each spectrum within each energy window depends primarily on (i) the concentration and interference of the radioactive elements; (ii) Compton scattering and the linear attenuation coefficient appropriate to the rock material and the energies of the transmitted gamma rays; (iii) the detector sensitivity and background count rate.

Besides the method of the three energy windows, the radioelement concentrations can be inferred from the total energy spectrum by means of the response matrix method (Matsuda et al. 2002). This technique consists of  $22 \times 22$  elements with unequal energy and pulse height intervals and is applicable to an energy range of 0–3.2 MeV for an isotropic field. Moreover, as the matrix is normalized at the ratio of the count rate to the incident photon fluence rate, one can obtain the flux densities directly from the pulse height distribution if the measured fields are isotropic.

Several factors may affect the accuracy of the determinations of  $^{40}\text{K}$ ,  $^{238}\text{U}$  and  $^{232}\text{Th}$  concentrations. Self-absorption due to the density variation in the rock samples seems of negligible importance, and tests on the energy calibration reveal good stability (a maximum drift of 3–4 channels only). Therefore, the main cause of error should lie in the uncertainty of the net count rate. In common rocks the relative standard uncertainty is minimum for potassium (1.2 %), maximum for uranium (3.5 %) and amounts to 2.4 % for thorium. For ultrabasic rocks with exceptionally low radioelement concentration the error increases to 20 %. The experimental standard deviations in carrying out repeated measurements are of the same order of magnitude (Watt and Ramsden 1964; Rybach 1988; Chiozzi et al. 2000a). In a 5400 s time lapse, a typical detection limit is estimated to be of 0.1 ppm for uranium, 0.2 ppm for thorium and 0.02 % for potassium.

### 2.5.2 Secular Equilibrium

Secular radioactive equilibrium in the decay series (see Faure 1986) is necessary to achieve reliable gamma-ray spectrometry measurements. This condition generally holds in the  $^{40}\text{K}$  and for  $^{208}\text{Tl}$  in the  $^{232}\text{Th}$  series, while problems may arise for  $^{214}\text{Bi}$  in the uranium series, where a minimum age of 0.3 Myr is required for  $^{226}\text{Ra}$  to be in equilibrium. In young rocks, this problem can be overcome by investigating the gamma-ray spectrum region comprised between 0.03 and 0.10 MeV, instead of the higher energy photo-peak of  $^{214}\text{Bi}$  (1.76 MeV) (Ketcham 1996). Chiozzi et al. (2002) tested this approach on young volcanic rocks by comparing results from the NaI(Tl) spectrometer with a germanium detector, and they found out that the use of the low energy window can remarkably reduce the uncertainty in the uranium determination. In this low-energy region, there are a number of gamma rays produced by the decay of  $^{234}\text{Th}$ . This radioelement can be safely assumed to be in secular equilibrium with  $^{238}\text{U}$  as its half-life is of only 24.1 days, and therefore could have a different activity from post- $^{226}\text{Ra}$  daughter products, like  $^{214}\text{Bi}$ . As the scintillation detector does not have a sufficient resolution to reliably distinguish individual peaks in this low-energy region, it is necessary to operate with a relatively wide window, ranging from 0.010 to 0.123 MeV.

### 2.5.3 Ground Spectrometry

Hand-held gamma-ray spectrometry is widely used in mapping surveys aiming at estimating concentrations of U, Th and K of surface rocks (Fig. 2.9). The instrument usually consists of a thallium-activated sodium iodide scintillation detector of about 440 cm<sup>3</sup> together with a photomultiplier tube, a high-voltage supply and a signal preamplifier. The probe is connected to a multichannel analyzer. Like in lab measurements, the determination of these elements is based on the method of the three energy windows (Chiozzi et al. 1998, 2000b).

Field instruments are calibrated by means of standard spectra acquired on three concrete pads enriched in K, U and Th, and with highly unbalanced K/U, Th/U and K/Th ratios. Ideally, calibration pads should simulate a geological source of radiation and should be kept dry, as variation in moisture content may lead to a change in radiation output. Pads are usually of cylindrical shape, with a diameter of 2–3 m and thickness of 0.5 m (IAEA 1989). A fourth, low-radioactivity calibration pad of lead is customarily used to measure the background.

Practically, the calibration procedure consists of measuring the net count rate at each window for each pad, which has finite dimensions and may differ from the recommended size. Grasty et al. (1991) showed that smaller transportable pads are also suitable for calibrating portable gamma-ray spectrometers, provided that a geometrical correction factor, derived from these calibration experiments, is applied to the instrument sensitivity. Furthermore, the detector must be set at a few

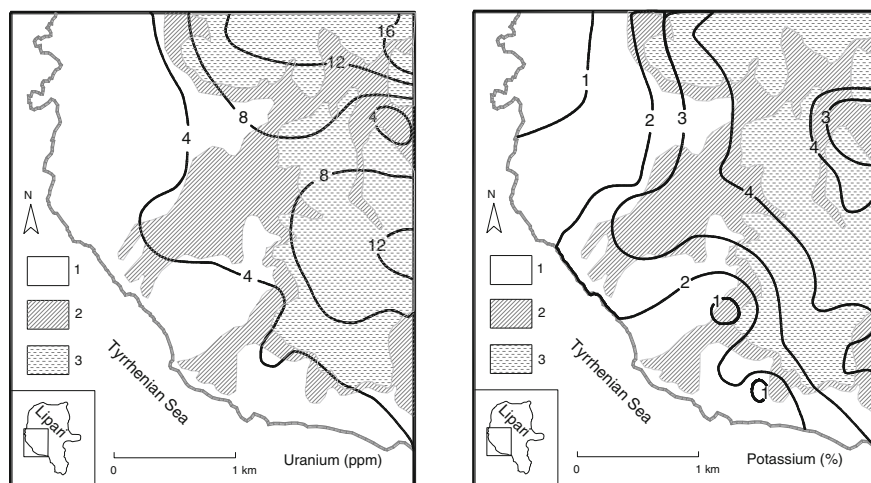


**Fig. 2.9** Ground radiometric survey in Lipari, Aeolian volcanic arc, Italy (modified after Chiozzi et al. 2007). Basaltic andesite to high-K andesite (from 223 to 127 kyr ago) (1); high-K andesite (from 127 to 92 kyr ago) (2); rhyolite (from 92 kyr to 1425 yr ago) (3)

centimeters from the surface. In such conditions the count rates are lower than those expected for a  $2\pi$  infinite geometry. Therefore, the recorded spectra must be corrected for a geometric factor  $G = 1 - 2h/d$ , where  $h$  is the height of the detector to the pad surface and  $d$  is the diameter of the standard pad. Usually the determination of the spectrometer sensitivity (with  $h = 63$  mm) is based on standard pads of 2 m in diameter (see e.g. Chiozzi et al. 2000b, for details). Under these conditions, the recorded gamma rays are those emitted from a rock volume of about  $1 \text{ m}^3$ . In underground measurements, such as in a mine gallery, gamma rays emitted from the walls and the vault are also revealed by the detector. This implies an increase in the count rate and, consequently, in concentrations. For a homogeneous and isotropic medium and a  $4\pi$  geometry, measured radioisotope concentrations are expected to double (Bochiolo et al. 2012).

The sampling time required for a measurement depends on the radioactivity of the rock and on the precision required. Lovborg and Mose (1987) derived equations giving the counting time for assays of each radionuclide with a 10 % error at various K, U and Th ratios. In practice, for NaI(Tl) detectors, IAEA (2003) recommends a sampling time of 120 s for highly radioactive rocks and 360 s for low radioactivity outcrops. This implies detection limits of 0.2 and 0.3 ppm for U and Th, respectively, and of 0.03 % for K.

Several factors may affect accuracy in the determination of radioelements. Sources of bias could be inherent to the instrument itself (e.g. drift of energy calibration, calibration of the reference materials, K contamination of the photomultiplier tube) and of geological nature (self-absorption due to variations in rock

density, outcrop alteration and geometry). Based on counting statistics, in common rocks the relative combined standard uncertainty of the measured concentrations is of about 3 % for K, 5 % for Th and 8 % for U.

### ***2.5.4 Background Radiation***

The net count rate and, consequently, the concentration results depend on the background, i.e. the gamma radiation that does not originate from the rock. Background radiation may be due to the internal radioactivity of the instrument, cosmic radiations—which change with the geomagnetic latitude and elevation—and the atmospheric radon. Therefore, before starting a field radiometric survey, it is important to assess the local background.

Besides on the lead pad, the background can also be estimated by taking measurements on a small boat (preferably of fibreglass) over a lake or sea, at a few hundred meters from a possibly flat shore (Chiozzi et al. 2001; IAEA 2003). Since artificial sources are not always available and, of course, differ from natural conditions, outcrops with energy distributions of gamma spectra similar to those typically emitted from the standards and as close as possible to a  $2\pi$  geometry can represent an alternative calibration site. Also serpentinitic rocks are a suitable source of background radiation, as their content of K, U and Th is nearly negligible (below the detection limit) (Chiozzi et al. 2000b). The background count rate generally increases with elevation. This is particularly evident in the  $^{40}\text{K}$  window. The overall effect is relatively small, but a correction for elevation is often incorporated to improve accuracy (Verdoya et al. 2001).

### ***2.5.5 Alteration Processes***

Secular disequilibrium in the U decay series can also be a consequence of alteration processes. On altered rocks, using the low-energy region of the gamma-ray spectrum allows to bypass this problem (see Sect. 2.5.1). Frequently, young volcanics are characterized by hydrothermal activity, which often implies kaolinization. This process yields a group of clay minerals dominated by kaolinite  $\text{Al}_2(\text{OH})_4\text{Si}_2\text{O}_5$  (in oxides  $\text{Al}_2\text{O}_3 \cdot 2\text{SiO}_2 \cdot 2\text{H}_2\text{O}$ ), a mineral which belongs to the group of aluminum silicates. Highly-altered argillic zones are often associated with sulphate-acid thermal springs.

The presence of hydrothermally altered zones, where strong remobilization of radioelements is to be expected, conditions the procedure of the radiometric survey, which thus requires both field and laboratory measurements. The detailed study of the spatial distribution and ratios of the radioelements provides a baseline for evaluating the depletion/enrichment processes, which may have affected altered rocks. Field spectrometry can put into evidence low radioactivity levels

near the altered zones. The lowest values of K usually occur at kaolin deposits and near hot springs. This is due to the K-depletion process which transforms feldspars and feldspathoids into kaolin.

Kaolinisation takes place in presence of  $H_2O$ ,  $CO_2$  and high temperatures. In particular,  $H_2O$  makes possible, by hydrolysis, the substitution of the alkaline and ferrous-alkaline cations in the form of base. At the same time,  $CO_2$ , soluble in  $H_2O$ , facilitates the transformation of the bases in soluble carbonates that are taken away definitively. Because of these reactions, feldspars and feldspathoids are transformed into colloidal silica and micaceous minerals of the sericite group; the latter can, in turn, lose other silica, and transform by oxidation into clayey minerals, such as illite and kaolinite. When the anhydrous aluminum silicates, which are found in feldspar-rich rocks, are altered by weathering or hydrothermal processes, kaolin is formed (Boulvais et al. 2000; Tourlière et al. 2003; Chiozzi et al. 2007).

Uranium and thorium are commonly fractionated during surface processes due to the oxidation of U into the soluble uranyl ion. The relatively immobile Th tends to concentrate and consequently the Th/U ratio should increase in altered rocks. However, in volcanic areas subject to hydrothermal processes such a ratio shows small variations, giving evidence for a proportional depletion of U and Th.

### ***2.5.6 Radioelement Concentrations and Heat Production***

Table 2.5 shows a compilation of concentrations of U, Th and K of a wide set of sedimentary and crystalline rocks, and the radiogenic heat calculated from (2.16). Rock types are sorted according to their depositional environment or to the tectonic regime in which they were formed. Ophiolites, amphibolites, conglomerates and breccias show the lowest concentrations of radionuclides. In general, U and Th are almost always below 1 ppm, and K is lower than 0.7 %. The highest U and Th concentrations are found in metamorphic rocks which also present high concentration of K (migmatites, orthogneisses and micaschists). Th concentration is below the detection limit in lherzolites, prasinites, serpentinites and opicalcites. In sedimentary and metasedimentary rocks, the average U content is maximum in dolomites, whereas the largest concentrations of Th and K are found in shales and cherts.

Apart from dolomites (which have an anomalous enrichment of U), ophiolitic complex rocks, some limestones, marls, conglomerates and breccias, the Th/U ratio is close to the value expected for a normal continental crust, ranging from 2.3 to 5.4. The estimated radiogenic heat is of course lower in the rocks with lower uranium and thorium concentrations. Excluding amphibolites ( $0.30 \mu W m^{-3}$ ), the largest radiogenic heat is found in metamorphic rocks ( $2.3\text{--}3.1 \mu W m^{-3}$ ). In sedimentary rocks, the radiogenic heat is maximum in shales, cherts, phyllitic schists and calc-schists ( $2.0\text{--}2.6 \mu W m^{-3}$ ).

**Table 2.5** U, Th and K average concentrations, Th/U ratio and radiogenic heat  $A$  in rocks of the Ligurian Alps (Italy) (after Chiozzi et al. 2001; Verdoya et al. 2001)

Tectonic/ sedimentary environment	Age	Rock type	<i>n</i>	U ppm	Th ppm	K %	Th/U	<i>A</i> μW m <sup>−3</sup>	
Ophiolitic complex	Middle-late Jurassic	Metagabbro	31	0.3	0.3	0.29	1.00	0.14	
		Metabasalt	23	0.4	0.3	0.52	0.75	0.19	
		Serpentinite schist	41	0.5	<0.3	0.08	0.60	0.16	
	Jurassic	Lherzolite	10	<0.2	<0.3	<0.03	1.50	0.08	
		Prasinite	12	0.4	<0.3	0.51	0.75	0.18	
	Middle Jurassic	Ophicalcite	10	0.4	<0.3	0.24	0.75	0.15	
		Metaophiolite	12	0.6	1.3	0.37	2.17	0.27	
	Pelagic siliceous sediments	Late Jurassic	Chert	10	3.2	15.2	5.14	4.75	2.20
		Jurassic	Quartz-schist	16	1.2	6.5	1.79	5.42	0.93
Shelf sediments	Middle-late Triassic	Dolomite	15	5.6	0.5	0.17	0.09	1.49	
Pelagic sediments	Early Cretaceous	Limestone	14	2.2	5.2	1.25	2.36	1.04	
	Lias	Limestone	13	2.6	3.8	1.11	1.42	1.04	
Pelitic-pelagic sediments	Early-middle Cretaceous	Phyllitic schist	10	3.0	13.3	3.07	4.43	2.00	
		Phyllite	20	2.9	10.6	2.52	3.36	1.73	
	Jurassic	Calc-schist	20	3.0	13.3	3.18	4.43	2.01	
	Pliocene	Marl	10	2.7	5.5	1.37	2.04	1.21	
	Dogger	Calcareous shale	10	2.8	10.1	2.41	3.61	1.66	
	Flysch	Late Cretaceous	Shale	15	4.1	16.7	3.60	4.07	2.57
Early Eocene		Marly limestone	10	1.8	4.2	1.15	2.33	0.87	
Molassic deposit	Middle Cretaceous	Shale	15	2.6	8.5	1.61	3.27	1.42	
		Arenaceous marl	10	2.4	8.8	2.19	3.65	1.45	
	Eocene	Conglomerate	10	1.1	1.6	0.43	1.45	0.42	
		Breccia	10	0.4	0.3	0.14	0.75	0.14	
Metamorphic	Pre-Carboniferous	Orthogneiss	94	4.1	17.6	4.23	4.29	2.65	
		Paragneiss	38	3.1	16.8	3.47	5.42	2.30	
		Migmatite	6	6.1	16.8	3.83	2.75	3.13	
		Amphibolite	31	0.5	1.2	0.69	2.40	0.30	
		Micaschist	30	4.1	17.5	3.92	4.27	2.66	

$n$  is the number of measurements

Table 2.6 shows an example of the radiogenic heat of rocks belonging to a young volcanic arc and the relative contribution of U, Th and K. The U concentration in rhyolites is remarkably higher than values commonly reported in the literature. The contribution due to U is about one half (44–52 %), whereas that of Th varies from 38 to 44 %. The larger values pertain to trachytic and rhyolitic rocks. The largest contribution yielded by K (about 16 %) is observed in mafic

**Table 2.6** Radiogenic heat  $A$  of volcanic rocks of the Aeolian arc (Tyrrhenian Sea) and the contribution supplied by each radioelement (after Verdoya et al. 1998a; Chiozzi et al. 2002)

Rock type	$A_U$ %	$A_{Th}$ %	$A_K$ %	$A$ $\mu W\ m^{-3}$
Basalt	43.7 (4.4)	38.4 (7.5)	17.9 (3.0)	0.6 (0.1)
Basaltic andesite	44.9 (4.2)	39.0 (5.7)	16.1 (2.7)	1.1 (0.6)
Andesite	45.7 (4.8)	39.4 (6.6)	14.9 (2.7)	1.3 (0.8)
Basaltic trachyandesite	48.1 (0.3)	43.2 (1.5)	8.6 (1.9)	4.3 (0.8)
Trachyte	52.0 (2.1)	43.0 (3.4)	5.0 (3.5)	7.1 (0.7)
Rhyolite	50.2 (0.7)	44.3 (1.2)	5.4 (0.6)	6.6 (0.9)

Standard deviation in parentheses

rocks. Basalts and andesites present typically low radiogenic heat values ( $0.6\text{--}1.3\ \mu W\ m^{-3}$ ), whereas trachytic and rhyolitic rocks denote values larger by a factor from six to ten ( $6.6\text{--}7.1\ \mu W\ m^{-3}$ ). Basaltic trachyandesites are characterized by an intermediate value ( $4.2\ \mu W\ m^{-3}$ ).

## 2.6 Radiogenic Heat in Depth

Experimental results on volcanic rocks show that the radioelement concentration and, consequently, the radiogenic heat are related to magmatic differentiation processes, thus implying a decrease with depth within the crust. The most widely accepted model is the exponential model by Lachenbruch (1970)

$$A(z) = A_0 \exp\left(-\frac{z}{D}\right) \quad (2.60)$$

where  $A_0$  (in  $\mu W\ m^{-3}$ ) is the radiogenic heat at the surface and  $D$  (in km) is the rate of heat decrease, which realistically explains the differences in the radiogenic heat of surface rocks in a region with a given tectonothermal history (heat-flow province) through the superficial erosion of radioisotopes. Factor  $D$ , which ranges from 5 to 15 km and is on average 10 km (Pasquale 1987), derives from the well-known linear relationship

$$q_o = q_a + A_0 D \quad (2.61)$$

where  $q_o$  is the heat flowing out from the Earth's surface, and  $q_a$  is a constant component of heat flow from the mantle. It is widely accepted that the surface radiogenic heat in the continental areas is of the order of  $3\ \mu W\ m^{-3}$ , as radioactivity measurements of igneous and metamorphic rocks restrict the actual range of radiogenic heat to  $2.5\text{--}3.5\ \mu W\ m^{-3}$ . Pasquale et al. (1990) suggested that radiogenic heat is related to the geological age  $t$  according to the empirical relation

$$A_0 = 3.2 \exp(-0.3t) \quad (2.62)$$

where  $t$  is in  $10^9$  years and  $A_0$  is in  $\mu W\ m^{-3}$ .

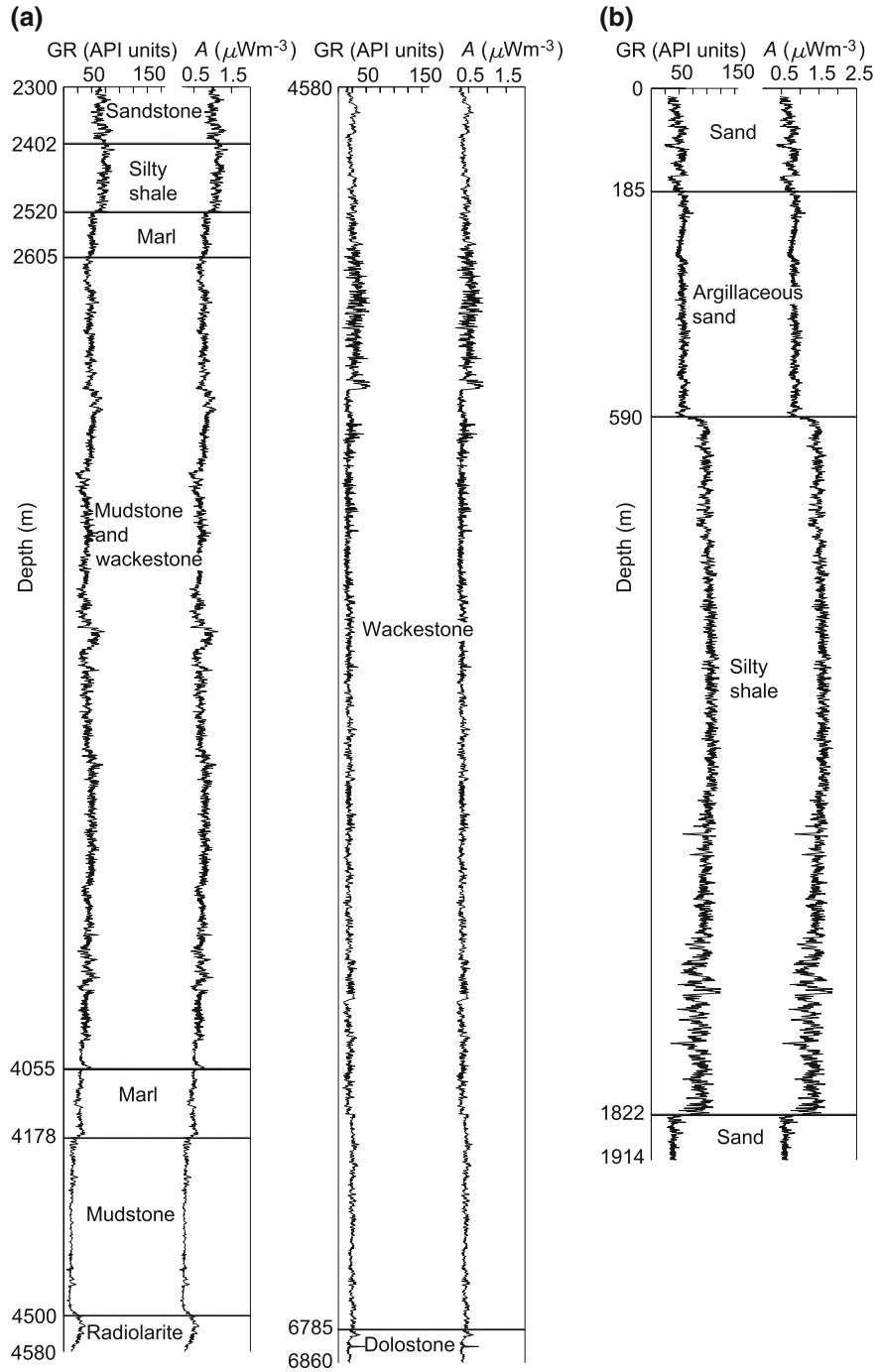


**Fig. 2.10** Radiogenic heat  $A$  derived from GR log of Chiari (a) and Carpaneto (b) wells, Po Basin (Italy)



**Table 2.7** Radiogenic heat  $A$  of rocks from GR logs and gamma-ray spectrometry (GRS) (after Pasquale et al. 2012)

Lithotype	$A$ ( $\mu\text{W m}^{-3}$ ) GR log	$A$ ( $\mu\text{W m}^{-3}$ ) GRS
Sand	0.74 (0.13)	
Sandstone	1.05 (0.02)	
Siltstone		1.13 (0.12)
Shale/silty shale	1.33 (0.24)	
Marl/silty marl	0.92 (0.14)	1.30 (0.14)
Argillaceous sandstone		1.39 (0.23)
Argillaceous limestone	0.63 (0.14)	
Mudstone/wackestone	0.45 (0.22)	0.34 (0.25)
Dolostone	0.46 (0.32)	
Radiolarite	0.43 (0.09)	
Dacite		0.58 (0.21)
Acid tuff	2.19 (0.15)	
Basaltic tuff	0.47 (0.05)	

Standard deviation in parentheses

Surface radiogenic heat within sediments has not been thoroughly investigated. Information on sediment radiogenic heat can be inferred from petroleum wells. After applying a correction for well diameter, drilling mud density and logging tool eccentricity, gamma-ray logs make possible to estimate  $A$  in  $\mu\text{W m}^{-3}$  by means of the relationship (Bucker and Rybach 1996)

$$A = 0.0158 (\text{GR} - 0.8) \quad (2.63)$$

where GR is the log reading in API units. Equation (2.63) may be used for GR values lower than 350 API units and gives  $A$  within an acceptable error ( $<10\%$ ). Figure 2.10 depicts the GR logs and the radiogenic heat profiles for two example wells, whereas the average values of  $A$  of several sedimentary rocks are shown in Table 2.7.

At crustal depth, Rybach (1979) and Rybach and Buntebarth (1984) argued that radiogenic heat can be estimated from  $P$ -wave velocity  $v_p$ , as the gradients in seismic velocity are accompanied by gradients in radiogenic heat. By taking into account the geological age, the relationship between  $v_p$  in  $\text{km s}^{-1}$  and  $A$  in  $\mu\text{W m}^{-3}$  is

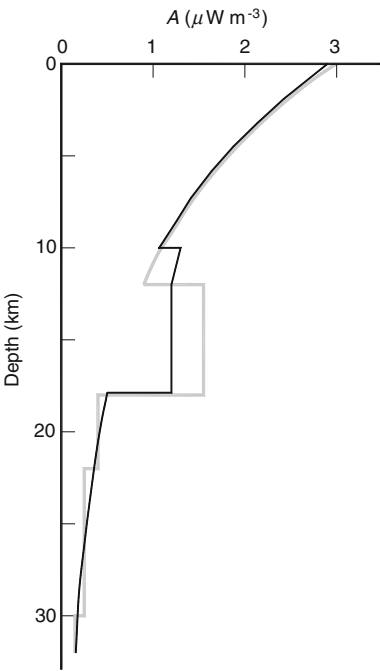
$$\ln A = B - 2.17v_p \quad \text{for } 6.0 < v_p < 8.2 \text{ km s}^{-1} \quad (2.64)$$

where  $B = 12.6$  for the Precambrian and  $13.7$  for the Phanerozoic crust. However, (2.64) takes for granted a simple lithological model of the crust, varying from acid to basic with depth, in agreement with the geochemical constraints. In crustal layers dominated by metamorphic rocks of complex evolution, such a relationship can lead to unreliable results (Kern and Siegesmund 1989).

**Table 2.8** Compositional model of the Variscan crust as inferred from the  $v_p(z)$  structure and the corresponding radiogenic heat  $A$  deduced from petrographical data (after Verdoya et al. 1998b)

Depth range (km)	Lithotype	Percentage of rock type	A (μW m <sup>-3</sup> )
<i>Upper crust</i>			
0–12	Granite-granodiorite	100	3.0
12–18	Granitic gneiss	55	1.6
	Granite-granodiorite	20	
	Tonalitic gneiss	25	
<i>Lower crust</i>			
18–22	Amphibolite	60	0.4
	Mafic granulite	40	
22–30	Mafic garnet granulite	65	0.3
	Amphibolite	35	
30–32	Mafic garnet granulite	100	0.2

**Fig. 2.11** Radiogenic heat  $A$  versus depth in the Variscan crust based on a compositional model (grey line) and the  $A$ - $v_p$  relationship (black line)



Other possible models of vertical distribution of radiogenic heat rely on both geophysical and petrographical constraints. Verdoya et al. (1998b) proposed an approach that allows the inference of a compositional model by combining crustal seismic profiles with  $P$ -wave velocity data of rocks from laboratory experiments (Fountain and Christensen 1989). A radiogenic heat value is assigned to each crustal layer on the basis of the compositional model (Table 2.8), and the

corresponding  $A(z)$  profile is obtained (Fig. 2.11). Equation (2.60) is applied to the granitic-granodioritic component down to a depth of 12 km, for values of  $D = 10$  km and surface radiogenic heat of  $3.0 \mu\text{W m}^{-3}$ . Below the uppermost granitic-granodioritic layer, the radiogenic heat is considered uniform with depth. Figure 2.11 also shows a comparison of the compositional model with a model based on (2.62) and (2.64). The radiogenic heat decreases versus depth according to  $D = 10$  km. In the lower crust,  $D$  was fixed by considering the  $A$  value at the top and the bottom of the layer. Below the Moho,  $A$  is assumed to be constant ( $0.01 \mu\text{W m}^{-3}$ ).

## References

- Abdulagatova Z, Abdulagatov IM, Emirov VN (2009) Effect of temperature and pressure on the thermal conductivity of sandstone. *Int J Rock Mech Min Sci* 46:1055–1071
- Balling NP (1976) Geothermal models of the crust and the uppermost mantle of the Fennoscandian shield in South Norway and the Danish embayment. *J Geophys* 42:237–256
- Beardsmore GR, Cull JP (2001) *Crustal heat flow: a guide to measurement and modelling*. Cambridge University Press, Cambridge
- Beck AE, Beck JM (1958) On the measurement of the thermal conductivity of rocks by observations on a divided bar apparatus. *Trans Am Geophys Union* 30:1111–1123 (Washington, DC)
- Beck AE (1988) Thermal properties. Methods for determining thermal conductivity and thermal diffusivity. In: Haenel R, Rybach L, Stegena L (eds) *Handbook of terrestrial heat flow density determination*. Kluwer, Dordrecht
- Benfield AE (1939) Terrestrial heat in Great Britain. *Proc Roy Soc London A* 173:428–450
- Birch F (1942) Thermal conductivity and diffusivity. In: Birch F, Schaier JF, Spicer HC (eds) *Handbook of physical constants*, vol 36. Geological Society of America, New York, pp 243–266
- Birch F (1950) Flow of heat in the front range Colorado. *Bull Geol Soc Am* 61:567–630
- Blackwell DD, Spafford RE (1987) Experimental methods in continental heat flow. In: Sammis CG, Henyey TL (eds) *Methods of experimental physics*. Academic Press, Orlando, Florida
- Bochiolo M, Verdoya M, Chiozzi P, Pasquale V (2012) Radiometric surveying for the assessment of radiation dose and radon specific exhalation in underground environment. *J Appl Geophys* 83:100–106
- Boulvais P, Vallet JM, Estéoule-Choux J, Fourcade S, Martineau F (2000) Origin of kaolinization in Brittany (NW France) with emphasis on deposits over granite: stable isotopes (O, H) constraints. *Chem Geol* 168:211–223
- Brigaud F, Vasseur G (1989) Mineralogy, porosity and fluid control on thermal conductivity of sedimentary rocks. *Geophys J* 98:525–542
- Bucher C, Rybach L (1996) A simple method to determine heat production from gamma-ray logs. *Mar Petrol Geol* 13:313–315
- Bullard EC (1939) Heat flow in South Africa. *Pro Roy Soc London A* 173:474–502
- Carslaw HS, Jaeger JC (1986) *Conduction of heat in solids*, 2nd edn. Clarendon Press, Oxford
- Čermák V, Rybach L (1982) Thermal conductivity and specific heat of mineral and rocks. In: Angenheister G (ed) *Landolt-Börnstein: numerical data and functional relationships in science and technology*. Springer, Berlin, pp 305–343
- Chiozzi P, Pasquale V, Verdoya M (1998) Ground radiometric survey of U, Th and K on the Lipari Island, Italy. *J Appl Geophys* 38:209–217

- Chiozzi P, De Felice P, Fazio A, Pasquale V, Verdoya M (2000a) Laboratory application of NaI(Tl) gamma-ray spectrometry to studies of natural radioactivity in geophysics. *Appl Radiat Isot* 53:127–132
- Chiozzi P, Pasquale V, Verdoya M, De Felice P (2000b) Practical applicability of field gamma-ray scintillation spectrometry in geophysical surveys. *Appl Radiat Isot* 53:127–132
- Chiozzi P, Pasquale V, Verdoya M (2001) Naturally occurring radioactivity at the Alps-Apennines transition. *Radiat Meas* 35:147–154
- Chiozzi P, Pasquale V, Verdoya M (2002) Heat from radioactive elements in young volcanics by gamma (Ray spectrometry. *J Volcan Geoth Res* 119:205–214)
- Chiozzi P, Pasquale V, Verdoya M, Minato S (2003) Gamma-ray activity in the volcanic islands of the Southern Tyrrhenian Sea. *J Environ Radioact* 67:235–246
- Chiozzi P, Pasquale V, Verdoya M (2007) Radiometric survey for exploration of hydrothermal alteration in a volcanic area. *J. Geochem Explor* 93:13–20
- Clark SP (1957) Radiative transfer in the Earth's mantle. *Trans Am Geophys Union* 38:931–938
- Clark SP (1966) Thermal conductivity. In: Clark SP (ed) *Handbook of physical constants*, vol 97. Geological Society of America Memoir, New York, pp 459–482
- Clauser C, Huenges E (1995) Thermal conductivity of rocks and minerals. In: Ahrens TJ (ed) *Rock physics and phase relations: a handbook of physical constants*. American Geophysical Union, Washington
- Cull JP (1975) The pressure and temperature dependence of thermal conductivity within the Earth. PhD Thesis, Oxford University, Great Britain
- De Vries DA, Peck AJ (1958) On the cylindrical probe method of measuring thermal conductivity with special reference to soils. *Aust J Phys* 11:255–271
- Deming D, Chapman DS (1988) Heat flow in the Utah-Wyoming thrust belt from analysis of bottom-hole temperature data measured in oil and gas wells. *J Geophys Res* 93:13657–13672
- Desai PD, Navarro RA, Hasan SE, Ho CY, DeWitt DP, West TR (1974) Thermophysical properties of selected rocks. Centre for Information and Numerical Data Analysis and Synthesis, Purdue University, West Lafayette, Indiana
- Drabble JR, Goldsmith HJ (1961) *Thermal conduction in semiconductors*. Pergamon Press, New York
- Fountain DM, Christensen NI (1989) Composition of the continental crust: A review, in geophysical framework of the continental United States. *Geol Soc Am Memoir* 172:711–742
- Grasty RL, Holman PB, Blanchard YB (1991) Transportable calibration pads for ground and airborne gamma-ray spectrometers. Energy, Mines, and Resources, Ottawa
- Grough ST (1979) Geoid anomalies across fracture zones and the thickness of the lithosphere. *Earth Planet Sci Lett* 44:224–230
- Hadglu T, Clinton CL, Bean JE (2007) Determination of heat capacity of Yucca Mountain stratigraphic layer. *Int J Rock Mech Min Sc* 44:1022–1034
- Hantschel T, Kauerauf AI (2009) *Fundamentals of basin and petroleum systems modelling*. Springer, Berlin
- Hashin Z, Shtrikman SA (1962) A variational approach to the theory of the effective magnetic permeability of multiphase materials. *J Appl Phys* 33:3125–3131
- Hasterok D (2010) Thermal state of the oceanic and continental lithosphere. PhD Thesis, University of Utah
- Hasterok D, Chapman DS (2011) Heat production and geotherms for the continental lithosphere. *Earth Planet Sci Lett* 307:59–70
- Hofmeister A (2005) Dependence of diffusive radiative transfer on grain-size, temperature, and Fe-content: implications for mantle processes. *J Geodyn* 40:51–72
- Horai K (1971) Thermal conductivity of rock-forming minerals. *J Geophys Res* 76:1278–1308
- Horai K, Simmons G (1970) An empirical relationship between thermal conductivity and Debye temperature for silicates. *J Geophys Res* 75:978–982
- IAEA International Atomic Energy Agency (1987) Preparation of gamma-ray spectrometry reference materials RGU-1, RGTh-1 and RGK-1. Technical Reports Series No. 148, Vienna

- IAEA International Atomic Energy Agency (1989) Construction and use of calibration facilities for radiometric field equipment, Technical Reports Series No. 309, Vienna
- IAEA International Atomic Energy Agency (2003) Guidelines for radioelement mapping using gamma ray spectrometry data. Technical Reports Series No. 1363, Vienna
- Joffe AV, Joffe AF (1958) Measurement of the thermal conductivity of semiconductors in the vicinity of room temperature. *Soviet Phys Tech Phys* 3:2163–2168
- Jessop AM (1990) Thermal geophysics. Elsevier, Amsterdam
- Kaganov MA (1958) A theoretical analysis of the method of measuring thermal conductivity of semiconductors proposed by A. V. Ioffe. *Soviet Phys Tech Phys* 3:2169–2172
- Kappelmeyer O, Hänel R (1974) Geothermics with special reference of application. *Geoexpl Monographs* Gebr Borntraeger, Berlin
- Kern H, Siegesmund S (1989) A test of the relationship between seismic velocity and heat production for crustal rocks. *Earth Planet Sci Lett* 92:89–94
- Ketcham RA (1996) An improved method for determination of heat production with gamma-ray scintillation spectrometry. *Chem Geol* 130:175–194
- Lachenbruch AH (1970) Crustal temperature and heat production: implications of the linear heat-flow relation. *J Geophys Res* 75:3291–3300
- Lawson AW (1957) On the high temperature heat conductivity of insulators. *J Phys Chem Solids* 3:155–156
- Lederer CM, Shirley VS (1978) Table of isotopes, 7th edn. Wiley, New York
- Lewis T, Villinger H, Davis E (1993) Thermal conductivity measurement of rock fragments using a pulsed needle probe. *Can J Earth Sci* 30:480–485
- Lovborg L, Mose E (1987) Counting statistics in radioelement assaying with a portable spectrometer. *Geophysics* 52:555–563
- Matsuda H, Minato S, Pasquale V (2002) Evaluation of accuracy of response matrix method for environmental gamma ray analysis (in Japanese). *Radioisotopes* 51:42–50
- Parrott JE, Stuckes AD (1975) Thermal conductivity of solids. Pion Ltd, London
- Pasquale V (1983) Sulla conducibilità termica delle rocce. *Convegno del Gruppo Nazionale di Geofisica della Terra Solida*, cnr, Roma, pp 765–775
- Pasquale V (1987) Possible thermal structure of the eastern part of the central Alps. *Nuovo Cimento* 10C:129–141
- Pasquale V, Casale G, Masella M (1988) Linear relationships between thermophysical properties and cation packing index of rocks. Preliminary results. *Convegno del Gruppo Nazionale di Geofisica della Terra Solida*, Cnr, Roma, pp 1423–1431
- Pasquale V, Cabella C, Verdoya M (1990) Deep temperatures and lithospheric thickness along the european geotraverse. *Tectonophysics* 176:1–11
- Pasquale V, Chiozzi P, Gola G, Verdoya M (2008) Depth-time correction of petroleum bottom-hole temperatures in the Po plain, Italy. *Geophysics* 73:E187–E196
- Pasquale V, Gola G, Chiozzi P, Verdoya M (2011) Thermophysical properties of the Po basin rocks. *Geophys J Int* 186:69–81
- Pasquale V, Chiozzi P, Verdoya M, Gola G (2012) Heat flow in the Western Po basin and the surrounding orogenic belts. *Geophys J Int* 190:8–22
- Popov YA (1983) Theoretical models of the method of determination of the thermal properties of rocks on the basis of movable sources. *Geol Prospect* 9:97–103 (in Russian)
- Popov YA, Pribnow D, Sass JA, Williams CF, Burkhardt H (1999) Characterization of rock thermal conductivity by high-resolution optical scanning. *Geothermics* 28:253–276
- Pribnow D, Sass JH (1995) Determination of thermal conductivity from deep boreholes. *J Geophys Res* 100:9981–9994
- Robertson EC (1988) Thermal properties of rocks. USGS open file report 88-441, US Geol Survey, Reston, Virginia
- Roy RF, Beck AE, Touloukian YS (1981) Thermophysical properties of rocks. In: Touloukian YS, Judd WR, Roy RF (eds) *Physical properties of rocks and minerals*. McGraw-Hill, New York

- Rybach L (1971) Radiometric techniques. In: Wainerdi RE, Uken EA (eds) *Modern methods of geochemical analysis*. Plenum Press, New York
- Rybach L (1979) The relationship between seismic velocity and radioactive heat production in crustal rocks: an exponential law. *Pure Appl Geophys* 117:75–82
- Rybach L (1988) Determination of the heat production rate. In: Rybach L, Stegena L, Haenel R (eds) *Handbook of terrestrial heat-flow density determination*. Kluwer, Dordrecht
- Rybach L, Buntebarth G (1984) The variation of heat generation, density and seismic velocity with rock type in the continental lithosphere. *Tectonophysics* 103:335–344
- Sass JH, Lachenbruch AH, Munroe R (1971) Thermal conductivity of rocks from measurements on fragments and its application to heat flow determinations. *J Geophys Res* 76:2291–3401
- Schärli U, Rybach L (2001) Determination of specific heat capacity on rock fragments. *Geothermics* 30:93–110
- Schatz JF, Simmons G (1972) Thermal conductivity of Earth materials at high temperatures. *J Geophys Res* 77:6966–6983
- Schloessin HH, Dvořák Z (1972) Anisotropic lattice thermal conductivity in enstatite as a function of pressure and temperature. *Geophys J R Astr Soc* 27:499–516
- Sekiguchi K (1984) A method for determining terrestrial heat flow in oil basinal areas. *Tectonophysics* 103:67–79
- Somerton WH (1992) *Thermal properties and temperature related behaviour of rock/fluid systems*. Elsevier, Amsterdam
- Somerton WH, Mossahebi M (1967) Ring heat source probe for rapid determination of thermal conductivity of rocks. *Rev Sci Instrum* 38:1368–1371
- Swann FG (1959) Theory of the AF Ioffe method for rapid measurement of the thermal conductivity of solid. *J Franklin Inst* 267:363–380
- Tourlière B, Perrin J, Le Berre P, Pasquet JF (2003) Use of airborne gamma-ray spectrometry for kaolin exploration. *J Appl Geophys* 53:91–102
- Tye RP (1969) *Thermal conductivity*, vol. 2. Academic Press, London
- Verdoya M, Pasquale V, Chiozzi P (1998a) Radioactive heat production of volcanics. In: *Proceedings of the international conference “The Earth’s thermal field and related research methods”*. Moscow, Russia, pp 272–276
- Verdoya M, Pasquale V, Chiozzi P, Kukkonen IT (1998b) Radiogenic heat production in the Variscan crust: new determinations and distribution models in Corsica (northwestern Mediterranean). *Tectonophysics* 291:63–75
- Verdoya M, Chiozzi P, Pasquale V (2001) Heat-production radionuclides in metamorphic rocks of the Briançonnais-Piedmont zone (Maritime Alps). *Eclogae Geol Helv* 94:213–219
- Von Herzen RP, Maxwell AE (1959) The measurement of thermal conductivity of deep-sea sediments by a needle probe method. *J Geophys Res* 64:1557–1563
- Wang J, Carson JK, North MF, Cleland DJ (2006) A new approach to modelling the effective thermal conductivity of heterogeneous materials. *Int J Heat Mass Transfer* 49:3075–3083
- Waples DW, Waples JS (2004a) A review and evaluation of specific heat capacities of rocks, minerals, and subsurface fluids. Part 1, minerals and nonporous rocks. *Nat Resour Res* 13:97–122
- Waples DW, Waples JS (2004b) A review and evaluation of specific heat capacities of rocks, minerals, and subsurface fluids. Part 2, fluids and porous rocks. *Nat Resour Res* 13:123–130
- Watt DE, Ramsden D (1964) *High sensitivity counting techniques*. Pergamon Press, London
- Zimmerman RW (1989) Thermal conductivity of fluid saturated rocks. *J Petrol Sc Eng* 3:219–227
- Zoth G, Haenel R (1988) Thermal conductivity. Methods for determining thermal conductivity and thermal diffusivity. In: Haenel R, Rybach L, Stegena L (eds) *Handbook of terrestrial heat flow density determination*. Kluwer, Dordrecht
- Faure G (1986) *Principle of isotopes geology*, 2nd edn. Wiley, New York

Geothermics

Heat Flow in the Lithosphere

Pasquale, V.; Verdoya, M.; Chiozzi, P.

2014, VIII, 119 p. 55 illus., Softcover

ISBN: 978-3-319-02510-0